Title: Age-dependent regulation of hippocampal inflammation by the mitochondrial translocator protein in mice

Running title: TSPO function in aging hippocampus

Authors: Kei Onn Lai[1], Jia Hui Wong[1], Nevin Tham[1], Lauren Fairley[1], Roshan Ratnakar Naik[1], Yulan Wang[1,2], Sarah R. Langley[3]*, Anna M. Barron[1]*

[1] Lee Kong Chian School of Medicine, Nanyang Technological University Singapore, Singapore. [2]Singapore Phenome Centre, Nanyang Technological University, Singapore 636921, Singapore. [3]School of Biosciences, Cardiff University, Cardiff, United Kingdom

*Correspondence to:

Anna M. Barron

barron@ntu.edu.sg

Lee Kong Chian School of Medicine

Clinical Sciences Building

11 Mandalay Rd, Singapore 308232

Tel: +65 6513 8028

Or

Sarah R. Langley

LangleyS2@cardiff.ac.uk

School of Biosciences

Cardiff University

Sir Martin Evans Building, The, Museum Ave, Cardiff CF10 3AX

Tel: +44 29225 14731

Abstract

The mitochondrial translocator protein (TSPO) is a biomarker of inflammation associated with neurodegenerative diseases, widely regarded to be upregulated in the aging brain. Here we investigated the interaction between aging and TSPO immunomodulatory function in the mouse hippocampus, a region severely affected in AD. Surprisingly, we found that TSPO levels were decreased in brain innate immune populations in aging. Aging resulted in a reversal of TSPO knockout transcriptional signatures following inflammatory insult. TSPO deletion drastically exacerbated inflammatory transcriptional responses in the aging hippocampus, whilst dampening inflammation in the young hippocampus. This age-dependent effect of TSPO was linked to NF-kβ and interferon regulatory transcriptional networks. Drugs that disrupt cell cycle and induce DNA-damage such as heat shock protein and topoisomerase inhibitors were identified to mimic the inflammatory transcriptional signature characterizing TSPO-dependent aging most closely. These findings indicate that TSPO plays a protective role in brain aging. This TSPO-aging interaction is an important consideration in the interpretation of TSPO-targeted biomarker and therapeutic studies, as well as *in vitro* studies which cannot model the aging brain.

1 Introduction

Aging is tightly associated with chronic inflammation, often termed "inflammaging", both of which are important risk factors for cognitive decline, dementia and delirium (Hou et al., 2019; Novoa et al., 2022). Inflammaging reflects age-related dysfunction in both peripheral and central immune function, leading to immune senescence, increased susceptibility to infection, and neuroinflammation. These inflammatory signals impair memory and cognition, and contribute to neurodegenerative diseases, including Alzheimer's disease (AD). Microglia, the resident innate immune cells of the brain, play a key role in brain aging and inflammation, becoming dysfunctional with age (Conde & Streit, 2006; Hefendehl et al., 2014; Lopes et al., 2022; Olah et al., 2018; Thomas et al., 2022). Aged microglia exhibit reduced proliferative capacity, chronic overactivity, increased proinflammatory cytokine release (Sierra et al., 2007; Ye & Johnson, 1999) and impaired phagocytosis, limiting clearance of misfolded protein aggregates that accumulate in the brain in aging and disease (Stuesse et al., 2000; Thomas et al., 2022). Aging also leads to systemic inflammation, resulting in increased circulating proinflammatory cytokines (Álvarez-Rodríguez et al., 2012), leakiness of the blood brain barrier (Hussain et al., 2021), with increased infiltration of inflammatory monocyte-derived macrophages (Silvin et al., 2022). These macrophages clustered at sites of neuropathology in AD (Silvin et al., 2022), and while other studies have associated markers of peripheral and brain inflammation with brain atrophy, cognitive decline and AD risk (Cullen et al., 2021; Liang et al., 2024). Consequently, how aging and inflammation, also known as inflammaging, intersect to increase risk of age-associated cognitive decline and neurodegenerative disease is an important question.

The translocator protein, or TSPO, is a useful molecular imaging target to visualize brain inflammaging in health and disease (Bradburn et al., 2019; Cagnin et al., 2001; Dani et al., 2018; Edison et al., 2008; Fan et al., 2015; Hamelin et al., 2016; Kreisl et al., 2013; Parbo et al., 2017; Schaum et al., 2020; Varrone et al., 2015; Versijpt et al., 2003; Yasuno et al., 2012; Yokokura et al., 2017). Using positron emission tomography, brain TSPO signals have been found to significantly correlate with age, AD pathology and cognitive deficits (Dani et al., 2018; Edison et al., 2008; Fan et al., 2015; Finze et al., 2023; Hamelin et al., 2016; Kreisl et al., 2013; Parbo et al., 2017; Pascoal et al., 2021; Versijpt et al., 2003). Although ubiquitously expressed, TSPO expression is upregulated in microglia and macrophages in response to inflammation (MacAskill et al., 2021; Nutma et al., 2021). For example, TSPO-PET has been used to image microglial inflammation in the human brain in response to systemic LPS administration (Sandiego et al., 2015).

A mitochondrial protein, TSPO is functionally important in microglial metabolic and immune responses. We and others have shown that genetic deletion of TSPO impairs microglial bioenergetics (Milenkovic et al., 2019) and phagocytosis, worsening pathogenesis in models of AD (Fairley et al., 2023; Pradhan et al., 2023; H. Zhang et al., 2021). Beyond its role in inflammation, TSPO has also been functionally implicated in aging, with a recent genetic study in drosophila showing that glial TSPO enhances longevity (Jullian et al., 2024). Functionally, TSPO has been implicated in the control of cellular bioenergetics (Hirsch et al., 1989; Liu et al., 2017), reactive oxygen species production (Guilarte et al., 2016; Loth et al., 2020), mitochondrial calcium homeostasis (Gatliff et al., 2017), mitochondrial cholesterol flux (Taylor et al., 2014) and mitochondrial-nuclear signalling (Desai et al., 2020). At the molecular level, TSPO interacts with key metabolic and inflammatory pathways in microglia and

macrophages, NADPH oxidase, a regulator of redox balance (Guilarte et al., 2016; Loth et al., 2020) and NF-Kβ signalling, a major inflammatory pathway (Horiguchi et al., 2019; Zhao et al., 2011). TSPO-dependent regulation of redox via NADPH oxidase has been linked to mitochondrial calcium homeostasis (Gatliff et al., 2017), while TSPO-mediated mitochondrial cholesterol flux has long been thought to play a role in steroidogenesis, a function supported by recent genetic studies in microglia and AD models (Bader et al., 2019; Pradhan et al., 2023). Interestingly, TSPO-mediated cholesterol flux has also been linked to NF-κB activation via retrograde mitochondrial-nuclear signaling (Desai et al., 2020). Meanwhile other studies have found NF-κB to be a upstream regulator of TSPO expression in microglia (Da Pozzo et al., 2019). Together, these findings highlight TSPO as a critical regulator of mitochondrial homeostasis, redox balance, and immune function, linking metabolic processes to inflammatory signalling and neurodegenerative disease processes.

Given mitochondrial and metabolic dysfunction is a universal hallmark of aging (López-Otín et al., 2013), and increasing evidence indicates that mitochondrial metabolism plays a key role in coordinating immune processes (Fairley et al., 2021), TSPO may provide an interface between aging and inflammation at the mitochondria in brain innate immune cells. Here we investigated the potential interaction between TSPO immune function and aging in the mouse hippocampus, a region critically involved in memory and highly vulnerable to both AD and age-related cognitive decline. We used systemic LPS inflammatory stimulus to examine the role of aging in immune senescence, as LPS is well established model for age- and disease associated inflammation, mimicking both neuropathological and cognitive changes observed in age, dementia and delirium (Ang et al., 2023; Bahaidrah et al., 2022; Brown & Heneka, 2024; Kealy et al., 2020; Nishiguchi et al., 2024; Sultan et al., 2021; J. Zhang et al., 2021).

2 Materials and methods

2.1 Animals and treatments Young (3 months) and aged (20 months) wild type (WT, C57BL/6) and homozygous global TSPO knock out (TSPO-KO) mice (Barron et al., 2018) were used. All experiments followed the National Advisory Committee for Laboratory Animal Research guidelines and were approved by the by the NTU IACUC (# A0384). To induce inflammation, mice received i.p. injections of phosphate buffered saline (PBS) or lipopolysaccharide (LPS, 1mg/kg, L2880, Sigma Aldrich) for 4 days. Brains were harvested 24 hour post-injection. Mice were anaesthetized (120mg/kg sodium-pentobarbital) and cardiac perfused with ice-cold PBS before hemibrains were snap frozen in dry ice cooled 2-methylbutane and stored at -80 ˚C.

Cell cultures and treatments For primary mouse microglia cultures, postnatal day 1 WT mice were decapitated, their brains (n = 6) were dissected, with meninges and blood vessels removed. Tissues from 2 pups dissociated in 2.5% trypsin (37°C, 10 min), followed by DMEM-COM (DMEM + 10% FBS + 1% Pen-Strep) and DNase I (10 mg/mL). After centrifugation (1200 RPM, 4°C, 10 min), cells were triturated in DMEM-COM + GM-CSF (0.5 ng/mL) and plated in poly-L-lysine-coated T75 flasks. After 24 hours, the medium was replaced, and cells were cultured until confluency without media changes to allow microglial proliferation. Microglia were harvested by vigorous tapping, plated on poly-L-lysine-coated 96-well plates, and used 1 day post-plating.

For primary bone marrow-derived macrophage (BMDM) cultures, femur and tibia from aged WT (14 mo) and TSPO-KO (11 mo) mice were flushed with ice-cold HBSS through a 70 μm nylon cell strainer. Cells were centrifuged (200G, 4°C, 5 min), treated with red blood cell lysis buffer (5 min, RT), and washed with IMDM + 2% FBS. After centrifugation (200G, 4°C, 5 min), cells were resuspended in RPMI-COM (M-CSF, 1:50) and seeded in 12-well plates (1 mL/well). On day 4, fresh media (500 μL) was added, and on day 10, cells were trypsinized and replated onto 96-well glass-bottom plates for experiments.

2.2 Senescence-associated β-galactosidase (SA-β-Gal) assay and NF-Kβ immunocytochemistry Primary microglia or macrophages were pre-treated with vehicle, Entinostat (500nM, MedChemExpress, HY-12163), or Entinostat + Ro5- 4864 (Sigma Aldrich, C5174) for 22hr, followed by co-treatment with vehicle or LPS (100 ng/mL) for 2 hrs. For SA-β-Gal activity, cells were washed (PBS), incubated with senescence dye (Abcam, ab228562, 37°C, 1 hr), washed (assay buffer x 2), and fixed (4% PFA, 10 min, RT). After PBS washes (3×), cells were permeabilized (0.1% Triton X-100) and blocked (5% Bovine Serum Albumin, BSA + 0.2% Triton X-100, 1 hour). Cells were then labelled in primary NF-kβ antibody (Cell Signaling Technology, 8242, overnight, 4°C), washed (PBS, 3×), and incubated with Alexa Fluor 634 anti-rabbit secondary antibody (Invitrogen, A31576, 1 hour, RT). Cells were washed (PBS, 5 min), then Fluoroshield with DAPI (Abcam, ab104139, 1 : 3 PBS dilution) was added to each well.

2.3 Imaging and image analysis
Images were captured on Zeiss LSM 800 Confocal Microscope with Plan-Apochromat 63x 1.4NA Oil Objective. Nyquist sampling with 0.34μm z-stack step size and twice averaging mean settings were used. Images were processed in Imaris 9.9.1 (Oxford Instruments)using Gaussian Filter background subtraction based on the smallest object in that channel. Cell segmentation was performed using DAPI (nuclei)and NF-Kβ immunoreactivity (cell boundaries), with nuclei and cell surfaces exported. Heterochromatin foci were identified using

baseline subtraction of the DAPI channel. Batch statistics were calculated using vantage options, with manual curation to exclude dividing cells or those cut off frame.

2.4   Flow cytometry analysis of TSPO in innate immune cells from mouse brain Innate immune cell populations were isolated from mouse brains as previously described (Sheng et al., 2019; Wu et al., 2021). Briefly, hemibrains were first dissociated mechanically, and then, enzymatically in dissociation buffer (100 mg/mL Collagenase (Roche Applied Science, Basel Switzerland), 1.2 U/mL Dispase (Roche Applied Science, Basel Switzerland), and 20 Units/mL DNase I (Life Technologies) in IMDM with 2% FBS) for 30 min at 37°C. Single-cell suspensions were obtained by passing through a 19-guage syringe and a 40 μm cell strainer, then pelleted (350g, 5min, RT) and resuspended in 4 mL 40% Stock Isotonic Percoll (SIP). The gradient suspension (40% over 70% SIP) was centrifuged (10 min, 2800 rpm, RT, deceleration 4) to isolate the interphase layer, which was pelleted (600g, 5 min) for staining. Cells were fixed (4% PFA), permeabilized (0.1% Triton X-100), and Fc-blocked (anti-CD16/32) before staining with the following antibodies: CD11c (BD Horizon, clone: N418), CD11b (BioLegend,clone: M1/70), CD45 (BioLegend, clone: 30F11), F4/80 (BioLegend,clone: BM8), MHC II (BioLegend,clone: M5/114.15.2), CD11c (BioLegend, clone: HL3), TSPO (Abcam, 109497). Flow cytometry data were analyzed with FlowJo software (TreeStar).

2.5   RNAseq data generation & analysis Frozen hippocampi from WT and TSPO-KO mice (n = 4/group, sex-matched within each group) were used to generate the RNAseq data. A subset of this data, the 3-months old treatment groups, was previously analysed and published (Fairley et al., 2023). Hippocampi were dissected out of hemibrains at -20°C, homogenised immediately in Trizol and total RNA extracted. Chloroform (1:5 vol: vol) was added to the Trizol homogenate then centrifuged for 12000 rpm, 15 min. The aqueous phase was removed, and total RNA extracted using Qiagen RNeasy mini kit column according to the manufacturer's instruction. RNA quality and purity was checked using the Agilent 2100 Bioanalyzer with Agilent 6000 Nano Kit. Total RNA of the samples had a minimum of RIN 8.3 with an average of RIN 9 and above. OligodT mRNAseq stranded library was prepared using NEBNext Ultra library preparation kit and sequenced using Illumina HiSeqTM.

Quality control of the FASTQ files was performed using FASTQC (http://www.bioinformatics.babraham.ac.uk/projects/fastqc/). Transcripts were quantified and aggregated at the gene level using the Salmon pseudo-aligner 1.9.0 using the *Mus musculus* genome Ensembl release 99 reference genome. Differential expression analyses were performed using the *DESeq2* (Love et al., 2014) 1.36.0 R package and nominal p-values were corrected for multiple testing using Benjamini-Hochberg. Log_2 (fold change) (Log2FC) values were shrunk using the *ashr* 2.2-54 R package (Stephens, 2017) and thresholded at Log2FC ≤ 0.5 or Log2FC ≥ 0.5. Volcano plots of RNAseq were constructed using the *ggplot2* (Wickham, 2016) R package 3.5.0 in an R 4.2.3 environment.

For gene set enrichment, the fGSEA R package 1.24.0 (Gennady et al., 2021) was used ranking genes by the Wald statistic from the differential gene expression analysis. Enrichments were run against the Reactome collection genesets for *Mus musculus* using 10000 permutations.

2.6   RNAseq DEGlist overlap analysis Differentially expressed genes (DEG) lists generated from DESeq2 were compared against each other for significant non-random

associations using the GeneOverlap package (Shen, 2023) (version 1.34.0) from Bioconductor. Each DEG list was filtered for significance and either categorised into gene sets as upregulated (FDR<0.05 and LFC≥0.5) or downregulated (FDR<0.05 and LFC≤-0.5). Fisher's exact test was performed for each gene set where odds ratio represents strength of non-random association between two gene sets.

2.7   Deconvolution methods for the estimate of relative abundance of cell types
Estimation of brain cell type abundance (absolute mode, 100 permutations) was performed using CIBERSORTx (Newman et al., 2019). The reference signature was prepared from single cell RNAseq of WT mice hippocampus Zeisel dataset (Zeisel et al., 2015). The count matrix of this dataset was CPM (counts per million) transformed using Seurat version 4 package (Hao et al., 2024). The bulk mixture of our RNAseq count data was CPM transformed for the deconvolution (same transformation space as the reference signature) using EdgeR package (Robinson et al., 2010). Permutational univariate ANOVA was used to evaluate presence of group differences for each cell type (RVAideMemoire version 0.9-83-7 package), followed by Dunn test (rstatix version 0.7.2 package) with FDR-correction for post-hoc pairwise comparison.

2.8   Weighted Gene Co-expression Network
For the multiWGCNA (Tommasini & Fogel, 2023) analysis, the gene expression count matrix was first normalized with the DESeq2 'variance stabilizing transformation (VST)`. WGCNA network was then constructed on the VST transformed data, using soft power threshold of 7, along with the default settings in the other arguments. Eigengenes of each module were extracted for plotting. PERMANOVA (permutational multivariate ANOVA, Euclidean method, 9999 permutations) was performed using the expression data for members of each corresponding module through linear model containing main effects, genotype and age, and interaction term genotype:age as testing covariates. PERMANOVA was performed using vegan package version 2.6-4. Following PERMANOVA, post-hoc pairwise comparisons was performed using estimated marginal means (EMM) with the same linear model as PERMANOVA. Estimated marginal means was conducted through emmeans package (Searle et al., 1980) version 1.10.0. Module driver genes were identified by high intra-modular connectivity defined as >0.9 Pearson's correlation with the module Eigenene of that specific module. Using module driver genes as query input, protein-protein interactions within the input was retrieved via Network Analyst platform (Zhou et al., 2019) and STRING database (Szklarczyk et al., 2021) (settings: High confidence PPI >900/1000 score, zero-order direct interactions). The final network was pruned using Prize-collecting Steiner Forest (PCSF) algorithm to isolate high confidence subnetwork consisting of the minimal number of edges.

2.9   Transcriptional Motif Analysis
Members of module 5, the module exclusively upregulated in TSPOKO aged group, was used as input for findMotifs.pl function in HOMER (Heinz et al., 2010) Motif Analysis. Known enrichment of transcriptional motifs that are either 8 or 10bp, and -2000bp till +500bp from the transcriptional start site (TSS) of the input genes were identified against all known motifs (29786 motifs) within HOMER database. Cognate genes (transcription factors) of significantly enriched (BH<0.05) motifs were then extracted from the expression matrix. These transcription factors were then integrated as a protein-protein interaction (PPI) network with module 5 members using Network Analyst software (Zhou et al., 2019) and STRING database (Szklarczyk et al., 2021).

2.10   Connectivity Map Analysis
The Connectivity Map (CMap) database of drug-induced transcriptional profiles was downloaded from Clue.io (Subramanian et al., 2017)

updated in 2021). This database is made up of over 720,000 drug perturbation signatures, derived from treating more than 33,000 small molecule compounds on various cell lines, including Neural Progenitor Cell (NPC) and glioblastoma (GI1). The top 100 of the differentially expressed genes from the inflammaging comparisons of TSPO-KO were used as inputs, to query the drug CMap database. Differential Expressed Genes were filtered for significance (FDR<0.05) and are either Log2FC ≥0.5 or ≤ -0.5. From within the Library of Integrated Network-Based Cellular Signatures (LINCS) database, compounded-treated signatures derived from the NPC (11,195 signatures) and GI1 (2,117) cell lines were independently queried with the TSPO-KO inflammaging signature.

The sscMap algorithm (Zhang & Gant, 2008) was utilised to compute the connectivity score, due to its superior sensitivity (Lin et al., 2020; Tham & Langley, 2022). The connectivity score can range from –1 to +1, where a positive connectivity score indicates a transcriptional phenocopying effect of a drug with the query signature, while a negative connectivity score indicates a transcriptional reversal of the drug and query signatures. From the individual connectivity scores, signatures treated with the same perturbation ID (pert_id) were summarised by computing their mean connectivity score.

The significance of the score is determined by randomly permuting the gene composition of the query signature, 1,000 times, to generate the null distribution scores. A connectivity score is considered significant if the absolute connectivity score exceeds 99% of the absolute scores from the null distribution.

2.11 Nuclear magnetic resonance spectroscopy (NMR) Metabolomics Analysis Frozen hemibrains from young and aged WT and TSPO-KO mice (n = 4-5/group) were used for NMR analysis. Tissues were weighted, homogenized and extracted using methanol:Water (2:1) followed by centrifugation (13800 g). The pellet underwent a second extraction, and pooled supernatants were dried (Spin-Vac, Eppendorf, Germany). Extracted samples were resuspended in D_2O buffer (550 µL, pH=7.4) with 0.05% sodium 3-trimethylsilyl (2,2,3,3-^{2}H4) propionate (TSP) used as chemical shift reference. NMR spectra were recorded on a Bruker Avance III HD 600 MHz spectrometer with 5mm BBI Z-Gradient high-resolution probe. One dimensional NMR spectra were recorded using NOSEY pulse sequence (recycle delay-G1-90°-t1-90°-G2-tm-90°-acquisition) with water suppression both during recycle delay (4s) and mixing time (100ms). A total of 256 scans were collected into 64k data points with spectral width of 30 ppm at the temperature of 300k. A 90-degree pulse set ~11 µs and 4 dummy scan were used.

The spectra were manually phased and corrected for baseline distortion and subsequently imported to Amix (Bruker, Germany, version 3.9.15) and region between 0.5~10ppm were integrated with 0.003 ppm(1.8Hz) bucket. The water peak resonance (4.60-4.70 ppm) was removed from each spectrum and the spectra were normalized to their respective wet weight of brain tissues. The normalized data were then exported to SIMCA (SIMCA-P15 UMETRICS, Umea, Sweden) for statistical data analysis. Metabolite concentrations were calculated by integration of peak area and further analysed by univariate analysis.

NMR peak assignment was performed by comparison of literature (Abreu et al., 2021; Li et al., 2015; Wang et al., 2005) and some were confirmed with statistical total correlation spectroscopy (STOCSY) (Cloarec et al., 2005). A peak at 4.832 ppm was identified that was only present in the aged TSPO-KO mice. Since it is a singlet, two-dimensional NMR is

insufficient for the peak assignment. We employed STOCSY method which takes advantage of high correlation for peaks in the same molecule or in the same metabolic pathway (Cloarec et al., 2005). It showed high correlation with peak at 8.462, which is formic acid. The correlation suggests that peak at 4.832 could be formaldehyde, which undetectable in normal circumstances. To confirm this assignment, we searched online information. Formaldehyde in water presents structure of methanediol and it is a singlet with chemical shift ranging from 4.4-5.4 ppm (Automated Topology Builder and Repository Version 3.0, Methanediol | CH_4O_2 | MD Topology | NMR | X-Ray (uq.edu.au)).

Shifted log ($\log_{10} x+1$) transformation was performed on raw data from targeted NMR due to right skewness of the data and presence of multiple zero values. PLSDA (Partial Least Squares Discriminant Analysis) was conducted using MixOmics package version 6.22.0 (Rohart et al., 2017). Number of components selected for each corresponding PLSDA was based on the number which gives the least classification error rate for that specified factor (either genotype:age interaction term, main effects genotype or main effects age). Performance of PLSDA was evaluated using 50 repeats and 4-cross fold validation (folds selection based on 4-5 samples per fold). PLSDA plots were generated using MetaboAnalyst 6.0 (Xia et al., 2009). Permutational univariate ANOVA (999 permutations) with sample groups as covariate, followed by pairwise post-hoc dunn test was conducted for statistical comparisons. Statistical analysis of the NMR data was performed in an R environment, R 4.2.3 using RVAideMemoire package (Hervé et al., 2018) for permutational univariate ANOVA (version 0.9-83-7) and rstatix (Kassambara, 2023) for dunn test (version 0.7.2).

3   Results & Discussion

3.1   Aging-dependent transcriptional signatures characterized by inflammation in mouse hippocampus

We determined normal age-related transcriptional signatures in the hippocampus by comparing the hippocampal transcriptome between young adult (3mo) versus aged (18mo old) WT mice (WT: 167 differentially expressed genes (DEGs), 96 upregulated, 71 downregulated; FDR < 0.05, shrunken LFC > shrunken LFC ≥ 0.5 or ≤ -0.5; Fig. 1A; Supplementary table 1A). Functional enrichment analysis indicated aging was associated with increased inflammatory transcriptional signatures, where top pathways with upregulated genes included cellular defense response, defense response to gram positive bacterium, positive regulation of TNF superfamily cytokine production (Fig. 1B, Supplementary tables 1B,C). Top pathways with genes downregulated in aging included mesenchymal cell development and chemorepellent activity, which predominantly reflected an abundance of genes encoding semaphorins (*Sema3a,c,d,f,g,4a,c,g,5b,6a,b,7a*). Semaphorins play critical roles in adult hippocampal connectivity, plasticity, myelination and neurogenesis. Neuropeptide signaling pathway genes were also downregulated in aging, including neuropeptides involved in hippocampal learning and memory (*Ntsr1/2*), synaptic plasticity and neurotransmission (*Gal, Adcyap, Nrg1, Sstr1/2/5, Tenm1*) and stress responses (*Cartpt, Crh, Avp, Pnoc, Oprm1, Oprk1, Pmch*).

The hippocampal age-associated inflammatory response (inflammaging) partially overlapped with the inflammatory transcriptional response induced by LPS in young adult hippocampus (65/125 aging-associated upregulated DEGs overlapped with upregulated DEGs following LPS treatment, *p*<0.0001, odds ratio =56.5; Fig. 1C, Supplementary table 1D). These included genes involved in innate immune responses (*Nlrp3, Ifi204, Ifit3, Tlr2*), complement cascade (*C4b, C1qa/b/c, C1ra, C3, C3ar1*) and antigen presentation (*H2-D1/K1/Q6/7, Ncf1/2*). Reflecting this, top enriched aged-associated functional pathways were also pathways associated with LPS-induced inflammation (Fig 1B, Supplementary table 1E). This is consistent with previous studies which have described increases in antigen presentation and complement pathways in the aging brain (Cribbs et al., 2012; VanGuilder et al., 2011), hypothesized to be associated with increased priming of innate immune responses, and microglial tolerance and senescence in the aged brain (Costa et al., 2021).

LPS is widely used as a model for age- and disease-associated inflammation, since it induces cognitive impairment and mimics both neuropathological and cognitive changes observed in dementia and delirium (Ang et al., 2023; Bahaidrah et al., 2022; Brown & Heneka, 2024; Kealy et al., 2020; Nishiguchi et al., 2024; Sultan et al., 2021; J. Zhang et al., 2021). This may reflect common inflammatory transcriptional pathways upregulated in aging and by LPS, as found in the current study. Inflammation can impair critical processes such as neurogenesis, plasticity, and myelination, which are vital for hippocampal function, contributing to age and LPS-induced cognitive impairment (Cammarota & Boscia, 2023; Perez-Dominguez et al., 2019; Valero et al., 2014).

Interestingly, in the aged brain, we observed a minimal effect of LPS on transcription signatures measured by differential expression analysis (aged LPS vs aged vehicle treated mice: 9 DEGs; 7 upregulated, 2 downregulated; FDR < 0.05, shrunken LFC > shrunken LFC ≥ 0.5 or ≤ -0.5; Supplementary table 1F). Likewise, we observed a low number of differentially expressed genes between LPS treated young and aged mice (young LPS vs aged LPS: 34 DEGs, 8 upregulated, 26 downregulated; Figure 1D, Supplementary table 1G). This suggested that the heightened inflammatory state in the aged hippocampus may limit further

transcriptional responsiveness to LPS, as compared to the young adult, where a robust immune transcriptional response was detected relative to the low baseline levels of inflammation.

3.2 TSPO levels decline in innate immune populations in aging mouse brain

To determine the effect of aging on TSPO expression in innate immune populations in the brain, we measured TSPO levels by flow cytometry in microglia, monocytes and macrophages isolated from young and aged mouse brain. Intriguingly, despite heightened inflammatory signatures in aged hippocampus, TSPO expression decreased in all three innate immune cell populations with aging (n = 6-10 mice/group, three-way ANOVA, age main effect: F = 26.84, p < 0.0001; Fig. 1E). Additionally, the effect of LPS treatment on TSPO expression was age-dependent, as indicated by a significant age x LPS treatment interaction (F = 3.62, p = 0.04). While TSPO is widely regarded to increase in the aging brain due to inflammaging (e.g.Repalli, 2014), contrary to expectations, our findings show that TSPO protein expression declines in the innate immune cells of the aging mouse brain. This discrepancy may arise because most studies reporting an age-associated increase in TSPO have relied on *in vivo* PET imaging (Gulyás et al., 2011; Paul et al., 2019; Schuitemaker et al., 2012), which cannot differentiate between cell-type specific contributions to TSPO signals. Notably, endothelial cells are a strong contributor to TSPO-PET signals (Wimberley et al., 2021). Meanwhile, other studies in human cohorts report region-specific elevations in TSPO-signals, restricted to hypothalamic and thalamic regions (Butler et al., 2022; Cagnin et al., 2001; Kumar et al., 2012), while yet others have found no association between brain TSPO-PET signals and aging (Suridjan et al., 2014). In mouse models of AD, TSPO-PET signals in various brain regions, including the hippocampus, exhibit a U-shaped trajectory, peaking midlife before gradually declining with further aging (Brendel et al., 2017; Focke et al., 2019). LPS has been widely shown to induce TSPO expression in mouse microglia, monocytes and macrophages (Blevins et al., 2021; Nutma et al., 2023; Shimoyama et al., 2019) and in humans increased TSPO-PET signals are detected following LPS administration (Sandiego et al., 2015). However, our findings indicate that the effect of LPS on TSPO expression in innate immune cells may also be age-dependent. Together, our findings challenge the prevailing notion that TSPO expression increases in brain innate immune populations with aging and highlights the importance of cell-type-specific contributions, regional variability and methodological consideration when interpreting TSPO as a marker of inflammation in the context of aging.

3.3 Hippocampal inflammaging is TSPO-independent

To determine if age-dependent loss of TSPO could play a role in brain inflammaging, we investigated if genetic TSPO deletion alters age-associated inflammatory signatures. Our comparison of transcriptional signatures in hippocampus of aged WT and TSPO-KO mice revealed surprisingly little effect of TSPO-KO on transcription, with only 34 DEGs (24 upregulated, 10 downregulated; FDR < 0.05, shrunken LFC > shrunken LFC ≥ 0.5 or ≤ -0.5 Fig. 2A; Supplementary table 2A). This suggested age-associated hippocampal inflammation is largely TSPO-independent.

Measurement of innate immune cell populations isolated from the brain and quantified by flow cytometry revealed increased total brain microglia in young adult TSPO-KO mice, which were depleted age-dependently (n = 6-10 mice/group Two-way ANOVA, age x genotype interaction: F = 12.20, p = 0.026; FDR post hoc: WT young vs KO young p = 0.04, KO young vs aged p = 0.0006; Fig. 2B). In WT mice, aging had no significant effect on microglial numbers (WT young vs aged p = 0.63). In contrast, no effect of aging or TSPO deletion was observed on brain populations of infiltrating monocytes or monocyte-derived macrophages (monocytes two-way ANOVA, age main effects: F = 0.21, p = 0.81, genotype main effects: F = 6.11, p = 0.19; macrophage two-way ANOVA age main effects: F = 0.49, p = 0.71, genotype main effects: F = 5.88, p = 0.21; Fig 2B). These findings suggest TSPO-

deletion may result in an aged-dependent impairment of microglial proliferative capacity, which could reflect increased cellular senescence (Hayakawa et al., 2007; Miller & Streit, 2007; Sharaf et al., 2013; Streit et al., 2008; Tremblay et al., 2012).

Given that TSPO- and age-dependent effects were observed on microglial numbers, we next applied statistical deconvolution methods to estimate the cell-type specific contributions to age-associated transcriptional signatures from the hippocampal bulk transcriptomic data. These methods leverage reference gene expression profiles for various cell types in the mouse brain to estimate the relative proportion of the transcriptional signatures attributable to specific cell types. No changes in estimates of contributions of major hippocampal cell types was detected between WT and TSPO-KO conditions (interneurons, pyramidal neurons, oligodendrocytes, astrocytes, macrophages or endothelial-mural cells; Supplementary Fig 1). However, aging was associated with a significant decline in the estimated contribution of astrocytes, a glutamatergic pyramidal neuron subtype found in the subiculum (subiculum subtype), and post-mitotic pre-myelinating oligodendrocyte subtype (subtype 1) (astrocytes, main effect: age, F = 5.08, p = 0.04; interneuron subtype 15, main effect: age, F = 10.81, p = 0.006; oligodendrocyte subtype 1, main effect: age, F = 15.10, p = 0.005; subiculum pyramidal neurons, main effect: age, F = 5.45, p = 0.04; Supplementary Fig. 1). These findings indicate that although TSPO-deletion leads to age-dependent alterations in microglial numbers, it does not appear to drive driven broader microglia-mediated changes in hippocampal transcriptional signatures.

3.4   TSPO - aging interaction in inflammatory transcriptional responses in hippocampus

Next, we examined the effect of TSPO deletion on LPS-induced transcriptional responses aging. TSPO deletion was associated with robust transcriptional differences in the hippocampal inflammatory response in aged mice, with 1184 significant DEGs identified in aged TSPO-KO mice treated with LPS (FDR <0.05; Fig 2C, Supplementary Table 2B). Of these DEGs, 593 were upregulated and 182 were downregulated genes with a shrunken Log2FC of either ≥ 0.5 or ≤ -0.5, resulting in 593 upregulated and 182 downregulated genes (shrunken Log2FC ≥ 0.5 or ≤ -0.5 respectively; Fig 2C, Supplementary Table 2B). Gene set enrichment indicated a downregulation of genes belonging to pathways related to the GABAergic synapse, respirasome, ATP synthesis coupled electron transport and NADH dehydrogenase complex assembly and an upregulation of genes in pathways involved in immune responses including defense response to symbiont, cell activation involved in immune response, positive regulation of tumor necrosis factor (TNF) superfamily and interleukin (IL) IL-1β production, and response to IL-6 production (Fig. 2D, Supplementary Table 2C). This was surprising since in the young adult mouse hippocampus, we found the opposite effect of TSPO deletion on inflammatory responses, including a dampening of responses to TNF signaling (Fairley et al., 2023).

We directly tested the overlap between TSPO-KO-specific transcriptional signatures in the young (Fairley et al., 2023) versus aged inflammatory hippocampus. Aging resulted in a reversal of TSPO-KO transcriptional signatures following inflammatory insult. A significant overlap between young *upregulated* and aged *downregulated* differentially expressed genes (DEG) (p<0.0001, odds ratio =11.39; Fig 2E, Supplementary Table 2D), and young *downregulated* and aged *upregulated* DEGs was observed in the inflammatory TSPO-KO hippocampus (p<0.0001, odds ratio =46.10; Fig 2E, Supplementary Table 2D). Functional

annotation indicated genes that were upregulated in the young but downregulated in the aged inflammatory TSPO-KO hippocampus related to transmembrane and calcium ion transport and myelination. Meanwhile, genes that were downregulated in the young but upregulated in the aged inflammatory TSPO-KO hippocampus related to immune system processes, including phagocytosis, respiratory burst and superoxide production, complement pathway, cellular response to interferons (β, γ), regulation of TNF production and NF-kβ signalling. This indicated an interaction between TSPO and aging in inflammatory responses.

An interactive shiny app is made to show the overlapping members for each overlapping comparison for effects of aging, LPS-induced inflammation and TSPO deletion (https://keionnbarronlab.shinyapps.io/venn_TSPOaging/).

3.5 TSPO – aging interaction changes heterogeneity of hippocampal cell-type contributions to inflammatory transcriptomic signatures

To determine whether changes in innate immune cell composition, such as increased immune cell infiltration, contributed to the TSPO-aging interaction in inflammatory transcriptional responses, we quantified microglial, monocyte and monocyte-derived macrophage populations in the brains of young and aged LPS-stimulated WT and TSPO-KO mice. No significant effect of TSPO deletion or aging was observed on brain innate immune cell populations (n = 5-12 mice/group; Fig 2F). Of note, in contrast to baseline conditions, TSPO-KO did not affect microglial numbers under inflammatory conditions in either the young or aged mice. These findings suggest that the TSPO-aging interaction in inflammatory transcriptional signatures may not be driven by differences in peripheral immune cell infiltration or microglial proliferation. However, our analysis of innate immune cell populations does not account for region-specific changes or the heterogeneity of microglial and macrophage subtypes, which may contribute to the observed transcriptional differences in aged-TSPO-KO mice.

To better understand this in hippocampus, we further investigated cell-type specific contributions to the TSPO-aging interaction in inflammatory transcriptional signatures of the hippocampus using computational deconvolution methods. No changes in the estimated contribution of the major hippocampal cell populations were detected (interneurons, pyramidal neurons, oligodendrocytes, astrocytes, macrophages or endothelial-mural cells; Fig 2G-L). However, an age-related decrease in estimated contribution of a subtype of GABAergic interneurons (subtype 7) found in the hippocampal CA1 region, a glutamatergic pyramidal neuron subtype found in the subiculum (subiculum subtype), and a post-mitotic pre-myelinating oligodendrocyte subtype (subtype 1), were detected in LPS treated TSPO-KO but not WT hippocampus (Fig 2M; interneuron subtype 7: main effect: age x genotype, F = 28.44, p = 0.004; Dunn multiple comparison p = 0.009; pyramidal neuron subiculum subtype: age x genotype, F = 4.50, p = 0.05, Dunn post-hoc corrected for multiple comparisons young vs old TSPO-KO p = 0.02; oligodendrocyte subtype 1: age x genotype F = 8.53, p = 0.008, Dunn post-hoc corrected for multiple comparisons young vs aged TSPO-KO p = 0.045). These findings suggest that TSPO deletion may specifically impact hippocampal neuronal and oligodendrocyte subtypes, potentially contributing to the downregulation GABAergic synapse-related genes and the age-related decrease in myelination-related genes identified in aged TSPO-KO mice under inflammation (Fig 2C).

With respect to the immune cells, estimated microglial contributions revealed a decrease in a microglia subtype characterized by expression of *Hexb* in LPS treated, aged TSPO-KO mice (age x genotype F = 12.85, p = 0.002, Dunn post-hoc corrected for multiple comparisons p = 0.06; Fig 2N). While it did not reach significance after correction, this was surprising given that microglia are a key inflammatory mediator in the brain, and TSPO-KO was associated with severely exacerbated transcriptional inflammatory signals in aging. The gene signature of this microglial subtype was enriched for pathways involved in cytokine-cytokine receptor interaction, osteoclast differentiation and phagosome (Supplementary Table 2E). Likewise, estimates of perivascular macrophage contributions did not significantly change across treatments (age x genotype F = 16.15, *p* = 0.059). However, interestingly, genes identifying a proangiogenic subtype of perivascular macrophages (subtype 2) were detected exclusively in aged TSPO-KO mice under inflammation. This was coupled with an increase in contributions of vascular endothelial cells subtype 1 (age x genotype F= 28.99, *p*=0.002, Dunn posthoc multiple comparisons TSPO-KO aged vs young *p* = 0.02, WT aged vs TSPO-KO aged *p*=0.03), which was enriched with genes involved in cytokine-cytokine receptor interaction pathways (Fig 2O). Both the perivascular macrophage and the vascular endothelial subtype that were increased in the TSPO-KO in inflammaging were enriched in cytokine-cytokine receptor interaction pathways. Analysis of the Zeisel dataset (Zeisel et al., 2015) indicated that these perivascular and endothelial populations express high levels of TSPO in adult wild type hippocampus, even compared to microglia, although their relative estimated abundance was far lower than microglia. This is in concordance with our analysis of TSPO protein expression, where macrophages were enriched with TSPO levels compared to microglia, although they represent <5% of all brain CD45+ cells. Upregulated TSPO expression in perivascular macrophages has been shown in a number of neuroinflammatory conditions including acute haemorrhagic leukoencephalopathy, viral infection and cerebrovascular disease (Victorio et al., 2024). In the context of cerebrovascular disease, TSPO upregulation in perivascular macrophages occurred independently of microglia (Nutma et al., 2023; Wright et al., 2020), suggesting that TSPO expression and function may potentially be regulated in an immune cell type and disease specific way. Future studies could address the cell specific immune functions of TSPO in these cell populations using conditional knockout mouse models.

3.6   TSPO - aging interaction linked to transcriptional control of NF-kβ and interferon regulatory factors (IRFs)

To describe systems-level transcriptional variation and identify discrete gene co-expression patterns associated with aging and TSPO deletion, we used a multi weighted correlation network analysis (multiWGCNA). This approach allows us to identify genes which cluster by their expression patterns across datasets with a temporal aspect. These clusters are termed gene co-expression modules. Gene co-expression provides insight into relationships between genes that can be used to identify regulatory networks, biological pathways and processes. WGCNA has proven to be a powerful method for identifying regulatory networks and functional pathways linked to biological processes such as aging (Holtman et al., 2015; Langfelder & Horvath, 2008). In our dataset, thirteen gene co-expression modules were identified (Fig 3A, Supplementary Table 3A). The relationship between these co-expression modules was evaluated by examining the inter-module higher organization, with strongly correlated modules organized into a network based on connectivity (Fig. 3A). Module interconnectivity suggests coordinated coregulation of modules. Of these, modules 6, 9 & 12 exhibited high connectivity within a network, as did modules 3-5 and 0,7, 8, 10 & 11;

suggesting coordinated co-regulation of these three sub-networks of modules. Gene Ontology overrepresentation analysis identified enriched functional terms associated with 9 of the modules within the network (Module 1,3-6, 8-10, 12; Fig 3A; Supplementary Table 3B). Module 1, which had low connectivity in the network suggesting independent regulation and function of this module, was functionally associated with synaptic maturation. Modules 6, 9 & 12, which exhibited a high degree of interconnectivity in the network, were enriched for terms related to immune function and responses, particularly innate immune response. Modules 3-5, which formed a separate subnetwork with a high degree of interconnectivity, were also enriched for immune related functions. Modules 8 & 10 which were in the third interconnected subnetwork were both functionally related to metabolic function. No significantly enriched functional terms were identified associated with module 0, 2, 7 or 11.

To identify which of these modules within the network were associated with aging and/or TSPO deletion, we then used factorial PERMANOVA analysis of multivariate gene expression for each module (Tommasini & Fogel, 2023). This approach enables module – multi-trait association for complex experimental design (main effects: age, genotype, age x genotype interaction). Six modules significantly differed across age and/or genotype (Modules 1-6; Supplementary Table 3A). This was reflected in the module-trait associations described below.

Modules 1 and 3 were age-associated co-expression modules. Module 1 was functionally associated with synaptic maturation, and contained 7724 downregulated genes in both aging and TSPO-KO conditions (PERMANOVA: main effect age: $p = 0.0001$, genotype $p = 0.0004$, genotype x age $p = 0.0032$; Supplementary Table 3A, B, Fig. 3B). This was consistent with previous aging studies showing age-associated downregulation of pathways related to synaptic maturation, plasticity and function in aging, which is thought to be a key factor in age-related cognitive decline (Smith et al., 2020). Interestingly, TSPO deletion exacerbated this age-associated depletion of synaptic transcriptomic signature in both young and aged mouse hippocampus.

Conversely, module 3, containing 1783 genes, was functionally associated with immunity and transcriptional and translational regulation; and was upregulated in both aging and TSPO-KO conditions (PERMANOVA: main effect age: $p = 0.004$, main effect genotype: $p = 0.0002$; Fig. 3C). Immune-related functional terms associated with module 3 included innate immunity and myeloid differentiation. These immune functions likely involved integrin-GTPase associate cell adhesion signalling processes, since *Itgb1* and *Cdc42* were identified as hub genes with the most protein-protein interactions (PPI) within a network constructed from the genes with high intra-module connectivity (module driver genes) (Supplementary Figure 2). Previous aging studies have also identified increased immune activation as a key signature in multiple regions of the aging brain (Ham & Lee, 2020). Meanwhile, transcriptional and translational regulatory functional terms in module 3 highlighted transcriptional elongation, regulation of RNA polymerase II promoter, and ribosome and ribonucleoprotein complex biogenesis (Supplementary Table 3B). Previous studies have shown age-related changes in transcriptional elongation and RNA splicing is associated with longevity across multiple organisms across different tissues including brain and that mutations that alter RNA polymerase II activity increase longevity (Debès et al., 2023). Within the PPI network, ribosomal genes involved in cell stress, cell cycle arrest and DNA damage were identified as hub genes, such as *Rps27a,* which has been identified as an early indicator of cell stress

(Supplementary Figure 2). Since these immune and transcriptional genes were identified as part of the same coregulated network, one possible explanation is these age-relate changes in immunity and transcription/translation are causally linked. Supporting this notion, several potential module driver genes were found to act as dual members of immune and transcriptional regulatory functional terms. These genes included *Lpxn, Zfp36, Lgals3, Elf1, Cd33*. Similar to observations in the synaptic maturation module, TSPO deletion exacerbated these age-related transcriptomic signatures of module 3, increasing expression in both young and aged mouse hippocampus. These findings indicate TSPO deletion exacerbates some synaptic and immune age-related transcriptional changes in the hippocampus.

Modules 4-6 were associated with the TSPO-aging interaction. Module 4, containing 443 genes, was identified as an immune module, associated with cytokine production and adaptive immune responses, and like module 3, the module genes were also upregulated in aging (PERMANOVA: main effect age: $p = 0.0004$; Supplementary Table 3B). Supporting the functional enrichment results, a PPI subnetwork of immune-related transcription factors and helicases including *Jak1/2, Stat3* and *Rela* were identified using the STRING database (Supplementary Figure 3). *JAK/Stat* are involved in cytokine signal transduction and response (e.g. interferons), while *Rela* is a transcription factor critical in NF Nuclear Factor Kappa B (*NF-kβ*) activation (Yu et al., 2004). Interestingly, this age-related increase of expression in module 4 was markedly exacerbated in the TSPO-KO condition (age x genotype: $p = 0.0045$, EMM post-hoc aged WT s aged TSPO-KO $p = 0.00013$; Fig. 3D, Supplementary Table 3A). Meanwhile another immune module (module 6, 223 genes), involved in viral responses and innate immunity, was downregulated in aging in WT, but upregulated in aging in TSPO-KO hippocampus (PERMANOVA: age x genotype p= 0.0001; EMM post-hoc: WT young vs old $p = 0.001$, TSPO-KO young vs old $p = 0.018$; Fig. 3E, Supplementary Table 3A-B). Immune pathways associated with module 6 included antigen processing and presentation, phagocytosis, necroptosis, regulation of NF-kβ signalling and response to interferons. Previous studies have demonstrated TSPO-PET can be used to visualize immune responses to viral infections (Shah et al., 2022). Our data suggests TSPO may play a role in dampening viral immune responses in aging hippocampus, and that this TSPO sensitivity to viral infections may be regulated by receptors involved in antigen presentation, given that the top 5 members with highest intramodulatory connectivity for module 6 were *Klhl21, Clec4a3, Gbp2, Trim30a, Iigp1* (Supplementary Table 3C).

An immune module that was functionally associated with response to bacterium and regulation of defense response (module 5, 371 genes) was of the highest interest amongst the coregulatory network because its genes were exclusively upregulated within the aged TSPO-KO group (PERMANOVA: age x genotype $p = 0.0001$; TSPO-Fig. 3D, EMM post-hoc aged TSPO-KO vs all other groups $p < 0.002$; Supplementary Table 3A-B). This module, like module 6, was enriched in genes functionally involved pathways that were downregulated in young but upregulated in aged TSPO-KO hippocampus. This included phagocytosis, respiratory burst and superoxide generation, TNF production and NF-kβ signalling. To predict potential transcription factors involved in regulating this TSPO-aging interaction, we leveraged transcription factor binding motifs in promoters (-500bp to +2000bp from TSS) based on the genes in this module (module 5; Fig 3G). Nine transcription factor motifs were significantly enriched (FDR <0.05; Supplementary Table 3D). A total of 20 cognate genes (transcription factors) of these motifs were found within the expression matrix. These were integrated as a protein-protein interaction network with module 5 members (Fig 3G). The *NF-kβ* transcription

factor, *Rela*, was identified as the hub node based on the highest degree connectivity (21 protein-protein interactions) and shortest average path (3.027) within the network (Supplementary table 3D). *Rela* was also identified as a hub in the PPI network of module 4, suggesting some overlapping regulatory pathways between these two modules. Additionally, most of the mapped transcription factors (13/20) in module 5 belonged to interferon transcription factors family (e.g *Irf1,Isg15*). Interestingly, *Spi1*, a macrophage-microglia transcription factor (Zhang et al., 2024), is predicted to interact with enriched interferon transcription factors (*Irf1,Irf4,Irf8*), suggesting that macrophage and/or microglia may be involved in mediating the interferon signalling network seen in module 5 (Fig 3G). Together, the integrated network of transcription factor-module 5 indicates that the immune pathways enriched within module 5 may be largely mediated by *NF-kβ* and interferon signalling. NF-kβ signalling was commonly identified between immune modules 4,5 and 6. Our results indicating a link between TSPO and *NF-kβ* is not an isolated finding. A previous study also identified NF-κB as a key signalling pathway mediating transcriptional changes following TSPO deletion in Leydig cells (Fan & Papadopoulos, 2021). Similarly, Desai *et al.* (2020) demonstrated that TSPO promotes NF-kβ activity by facilitating cholesterol redistribution to the nucleus through retrograde mitochondrial-nuclear signalling in breast cancer cells. Conversely, Da Pozzo *et al.* (2019) found that NF-kβ itself regulates TSPO expression, with a binding site identified in the *Tspo* promoter, suggesting a regulatory feedback loop, where elevated NF-kβ activity upregulates TSPO expression, which in turn acts to suppress NF-kβ activity. Our findings build upon this concept, indicating that NF-kβ is not only a downstream effector of TSPO, but also a key mediator of the TSPO-aging interaction in inflammation. Since *NF-kβ* and interferons have been identified as potential therapeutic targets in AD (Chavoshinezhad et al., 2023; Grimaldi et al., 2014; Mudò et al., 2019; Sun et al., 2022), and play an important role in driving inflammaging and senescence (Salminen et al., 2008; Salminen et al., 2012; Songkiatisak et al., 2022) the TSPO-aging interaction in *NF-kβ* and interferon transcriptional pathways may be an important consideration in therapeutic development.

3.7   Drugs that disrupt cell cycle and induce DNA-damage mimic TSPO-dependent aging transcriptional signature

To further investigate, we used an *in silico* approach to identify small molecules that phenocopy TSPO-dependent inflammaging. We compared the TSPO-dependent inflammaging transcriptome signature with drug gene expression signatures in a perturbational signature library called Connectivity Map (CMap), using the LINCS database (Tham & Langley, 2022). The similarity (or dissimilarity) between the TSPO-KO inflammaging and drug signatures is quantified with a connectivity score, where a score of +1 indicates a strong transcriptional phenocopy, while a score of –1 indicates a strong transcriptional reversal of the TSPO-KO inflammaging signature. We focused on transcriptional signatures from drugs screened in two key cell types: neural progenitor cells (NPCs) and a glioblastoma cell line (GI1). This approach can help identify drugs that can reverse pathological gene expression patterns and provides insights into mechanism of action by linking gene expression signatures from the aging TSPO-KO inflammatory condition with known drug signalling pathways.

CDK (cyclin-dependent kinase) inhibitors, topoisomerase inhibitors and heat shock protein 90 (HSP90) inhibitors were commonly identified in both cell types analysed to closely mimic the inflammatory transcriptional signature characterizing TSPO-dependent aging (Fig 4A, B). These drugs disrupt processes such as cell cycle regulation, DNA integrity and stress

response pathways, and can be used to induce cellular senescence. The highest ranked phenocopy compound identified in the NPCs, Dinaciclib (mean connectivity score = +0.33), is a selective inhibitor of the CDK1, CDK2, CDK5 and CKD9. This compound was not tested in the GI1 cell line. CDK inhibitors suppress the activity of key kinases at different stages of the cell cycle process thus halting cell proliferation (Parry et al., 2010; Webster & Kimball, 2000). Another selective CDK1 inhibitor, CGP-60474, is the 5th ranked phenocopying compound with TSPO-KO inflammaging (mean connectivity score = +0.30; Fig 4A). Likewise, a number of CDK inhibitors were also identified to significantly phenocopy the TSPO-dependent inflammaging signature in the glioma GI1 cells, although they were not the strongest phenocopies identified (Supplementary Table 4). While specific CDK inhibitors were not as strongly correlated with the TSPO-KO inflammaging signature in the GI1 glioma compared to the NPC, the top ranked phenocopy drug in the GI1 glioma cells is the CHK (Checkpoint) inhibitor, LY-2606368 (1st, +0.25). Checkpoint kinases are upstream regulators of CDKs (Janetka & Ashwell, 2009), corroborating potential disruption of cell cycle processes in TSPO-KO inflammaging.

Two Topoisomerase inhibitors, Mitoxantrone and Topotecan, also strongly phenocopied the TSPO-KO inflammaging signature in NPCs (ranked 2nd and 3rd, mean connectivity score = +0.32 and +0.31, respectively; Fig 4A). Although these two topoisomerase inhibitors were not tested in the GI1 glioma cell line, the inhibitors Daunorubicin (25th rank, mean connectivity score = +0.15) and Camptothecin (77th, +0.10) also significantly phenocopied the TSPO-dependent inflammaging signature (Fig. 4B). Topoisomerase inhibitors are DNA-damage inducing compound, that act by trapping the Top1-DNA cleavage complex (Top1cc) and preventing the cleaved DNA from re-ligating, typically used to trigger cancer cell apoptosis (Katyal et al., 2014). This potentially indicated elevated DNA-damage in TSPO-KO inflammaging hippocampus.

Interestingly, two heat shock protein 90 (HSP90) inhibitors were also highly ranked, phenocopying the TSPO-KO inflammaging signature — Tanespimycin (ranked 7th, mean connectivity score = +0.22) and Geldanamycin (ranked 10th, mean connectivity score = +0.20; Fig 3A). These compounds bind to the HSP90, which in turn releases the HSF1 (heat shock factor 1) transcription factor to activate the expression of other HSPs during cellular stress (Kurop et al., 2021). This finding suggests that cellular stress triggering the heat shock response may also be associated with the loss of TSPO function during inflammaging.

Overall, the classes of drugs found to mimic TSPO-dependent aging induced key hallmarks of cellular senescence, including cell cycle disruption and DNA-damage. Based on this, we hypothesized that TSPO-deletion in aging promotes innate immune cell senescence via NF-Kβ signalling, which we had identified as a hub in the TSPO-aging transcriptional networks. In subsequent studies we test this hypothesis in cultured microglia and macrophages.

3.8   TSPO modulates NF-kβ activation in microglia and macrophages

To test the hypothesis that TSPO-deletion promotes innate immune cell senescence in aging via NF-Kβ signalling, we investigated the effect of Entinostat, a histone deacetylase (HDAC) inhibitor, which was identified in our analysis to strongly phenocopy the TSPO-KO aging transcriptomic signature. Entinostat was selected for further investigation because it is known to effect NF-Kβ signalling pathways, innate immune activation and cellular senescence (Benjaskulluecha et al., 2022; Bhat et al., 2024; Dai et al., 2005; Min et al., 2021; Ryu et al.,

2019; Sidiropoulos et al., 2022; Stanfield et al., 2021). Of particular interest, a previous study has demonstrated that Entinostat enhances LPS-induced inflammatory responses in macrophages (Benjaskulluecha et al., 2022).

First, we established an *in vitro* model of aged microglia by treating primary microglia with Entinostat combined with LPS to induce cellular senescence. As a biomarker of cellular senescence, we measured β-galactosidase activity (SA-β-Gal), a hallmark of aging and senescent cells. Entinostat combined with LPS increased SA-β-Gal activity, which was not reversed by the TSPO agonist, Ro5-4864 (one-way ANOVA, F = 35.42, $p < 0.0001$, FDR posthoc, vehicle vs entinostat + LPS or vehicle vs entinostat + LPS + Ro5-4864: $p < 0.0001$; n = 96 – 135 cells/group; Fig. 4E). Notably, although the TSPO agonist did not alter total SA-β-Gal activity, it resulted in smaller, yet more abundant SA-β-Gal-positive lysosomes.

Next, we tested the effect of Ro5-4864 on nuclear localization of the NF-kβ subunit P65 in senescent microglia treated with Entinostat + LPS. Increased nuclear NF-kβ was observed in Entinostat + LPS treated microglia, which was reversed by Ro5-4864 (one-way ANOVA, F = 4.86, $p = 0.008$, FDR post hoc, vehicle vs. entinostat + LPS: $p = 0.006$; entinostat + LPS vs. entinostat + LPS + Ro5-4864: $p = 0.04$; n = 96 – 135 cells/group; Fig 4C, F). Increased nuclear NF-kβ in Entinostat + LPS treated microglia was couple with an increase in total cellular NF-kβ, while following Ro5-4864 treatment, reduced nuclear NF-kβ was observed despite further elevations in total cellular NF-kβ (one-way ANOVA, F = 20.25, $p < 0.0001$, FDR post hoc, vehicle vs. entinostat + LPS: $p = 0.04$; entinostat + LPS vs. entinostat + LPS + Ro5-4864: n = 96 – 135 cells/group; $p < 0.0001$; Fig 4C, F).

This was associated with morphological changes, as Ro5-4864 treated microglia appeared rod-like with fewer processes, which was reflected in significantly increased circularity in Ro5-4864 treated microglia (one-way ANOVA, F = 7.06, $p = 0.001$, FDR posthoc, entinostat + LPS vs entinostat + LPS + Ro5-4864: $p = 0.04$; n = 96 – 135 cells/group; Fig. 4D, F). These findings support a role for TSPO in modulating NF-kβ signalling in senescent microglia.

To genetically investigate the potential role of TSPO in NF-kβ signalling, we compared nuclear NF-kβ activation in primary macrophages derived from aged WT and TSPO-KO mice. We found that LPS (alone or in combination with Entinostat) robustly increased nuclear NF-kβ in TSPO-KO but not WT macrophages (one-way ANOVA, F = 3.92, $p = 0.0004$, FDR post hoc: WT vehicle vs LPS $p = 0.70$, TSPO-KO vehicle vs LPS $p = 0.02$; n = 55 -119 cells/group; Fig. 5A, D). Total cellular NF-kβ levels were not significantly changed between treatment conditions (one-way ANOVA, F = 1.88, $p = 0.07$; n = 55 -119 cells/group; Supplementary Fig. 4A,C). Macrophages treated with LPS and Entinostat, alone or in combination, appeared more ameboid, this was measurable in TSPO-KO macrophages treated with Entinostat + LPS, which had significantly increased sphericity compared to vehicle treated WT macrophages (one-way ANOVA, F = 2.31, $p = 0.03$; FDR post hoc: WT vehicle vs TSPO-KO entinostat + LPS $p = 0.03$; n = 55 -119 cells/group; Supplementary Fig. 4B). Surprisingly, Entinostat reduced senescence marker, SA-β-Gal, in TSPO-KO but not WT macrophages (one-way ANOVA, F = 3.75, $p = 0.0006$; FDR post hoc: WT vehicle vs WT Entinostat: $p = 0.39$, TSPO-KO vehicle vs TSPO-KO Entinostat: $p = 0.009$; n = 55 -119 cells/group; Fig 4B,C). This corresponded to reduced heterochromatin foci in Entinostat treated TSPO-KO but not WT macrophages, corroborating reduced senescence and suggesting Entinostat induced increased chromatin relaxation in TSPO-KO compared to WT macrophages (one-way ANOVA, F = 4.51, $p = 0.01$;

FDR post hoc: WT vehicle vs WT Entinostat: $p = 0.13$, TSPO-KO vehicle vs TSPO-KO Entinostat: $p = 0.02$; n = 8-12 images from 3 replicates/group; Supplementary Fig. 4C). LPS treatment increased senescence measured by SA-β-Gal activity in both WT and TSPO-KO macrophages treated with Entinostat.

3.9   Aging and TSPO alter brain metabolic profiles in inflammation

Since our transcriptomic data identified TSPO-dependent changes in metabolic pathways in the aged brain under inflammation, NMR was used to determine brain metabolites involved in metabolism of carbohydrates, amino acids and lipids in young and aged WT and TSPO-KO mice treated with LPS. We identified 20 metabolites which includes amino acids (glutamine, glutamate, aspartate, N-acetylaspartate (NAA), gamma-aminobutryric acid (GABA), tricarboxylic acid cycle (TCA) metabolites (fumarate, succinate), redox cofactors (NAD, Nicotinamide (NAM), Adenosine diphosphate (ADP) and membrane components, (choline, glycerophosphatidylcholine, Phosphatidylcholine) (Fig 6A). Additionally, a peak corresponding to formaldehyde, which is usually undetectable in brain, was identified exclusively in the aged TSPO-KO mice (Fig 6B).

PLS-DA was used to determine the major metabolites discriminating between young versus aged and WT versus TSPO-KO conditions (Fig 6C). Each group clustered with distinct separation by genotype for each age. Aging was most clearly discriminated along the principal component axis 1 and 2, which explained 41.1% and 15.9% of the variability, respectively (Fig 6C). Metabolites that contributed the greatest variance to discrimination of the groups along PC1 were involved in the TCA cycle (Fumarate, Succinate, Glutamate, GABA, Aspartate), membrane phospholipids (Phosphatidylcholine, Glycerolphosphocholine), and redox cofactors (NAD, NAM, ADP; Variance Importance Projections (VIP) score > 0.8 ; Fig 6A).

Comparison of metabolite concentrations in aging revealed increased levels of the TCA metabolite, succinate, coupled with reduced levels of its product, fumarate, suggesting inefficient conversion of succinate to fumarate in the aged inflammatory brain (PERMANOVA: main effect: aging; Fumarate, $F_{(1,5.66)} = 8.41$, $p = 0.007$; succinate, $F_{(1,5.66)} = 4.98$, $p = 0.043$; Fig 6D; Supplementary Table 5). Supporting this, succinate and fumarate levels were significantly correlated in young but not aged brains in both WT and TSPO-KO mice, suggesting a break in the TCA cycle at succinate dehydrogenase in aged mice (Fig. 6D). TSPO deletion was also associated with depleted levels of fumarate (PERMANOVA: main effect: genotype; Fumarate, $F_{(1,5.66)} = 5.82$, $p = 0.026$; Fig 6D, Supplementary Table 5). Further, age-related depletion of fumarate was more severe in TSPO-KO brains, with reduced levels detected in young and aged TSPO-KO mice compared to young WT (PERMANOVA: age x genotype interaction; Supplementary Table 5; fumarate, $F_{(3,5.66)} = 6.70$, $p = 0.003$; young WT vs aged TSPO-KO, FDR = 0.0067). Interestingly, fumarate is an anti-inflammatory metabolite, shown to inhibit activation of NF-κβ and approved for treatment of multiple sclerosis (Miljković et al., 2015). Therefore, depleted levels of this metabolite could potentially contribute to the increased inflammatory transcriptional signatures detected in TSPO-KO inflammaging.

Age-related reductions in levels of glutamate, which fuels the TCA cycle via α-ketoglutarate, in addition to being the major excitatory neurotransmitter of the brain, were also observed (PERMANOVA: main effect: aging; glutamate, $F_{(1,5.66)} = 5.70$, $p = 0.011$; Fig 6D; ; Supplementary Table 5). Glutamate concentrations significantly correlated with levels of its

precursor, glutamine in young but not aged brains of both WT and TSPO-KO mice, potentially indicating reduced efficiency of glutamate synthesis in the aging brain (Fig. 6D). In contrast, TSPO deletion resulted in significantly reduced levels of the glutamate metabolite, GABA, which feeds into the TCA cycle via succinate, in addition to being the major inhibitory neurotransmitter of the brain (PERMANOVA: main effect: genotype; GABA, $F_{(1,5.66)} = 6.02$, $p = 0.015$; Fig 6D; ; Supplementary Table 5). Depleted brain GABA levels in TSPO-KO mice was consistent with our transcriptomic findings, that identified a downregulation of pathways related to the GABAergic synapse in the hippocampus of aged TSPO-KO vs WT mice. These changes in glutamate and GABA levels could potentially reflect excitatory-inhibitory imbalance, which is associated with anxiety and depression (X. Zhang et al., 2021). We have previously shown that TSPO deletion increases anxiety-related behavior in mice (Barron et al., 2021), thus changes in bioavailability of glutamate and GABA may contribute to this effect.

Reduced accumulation of the energy substrate, ADP, was also observed in the aging brain (PERMANOVA: main effect: aging; ADP, $F_{(1,5.66)} = 4.65$, $p = 0.005$; Fig. 6D). ADP levels significantly correlated with concentrations of its metabolite, AMP, but not ATP, in the brains of young WT mice only. A significant interaction between TSPO-KO and aging was identified for ADP, with pairwise analysis indicating ADP was significantly reduced due to aging in WT mice only (PERMANOVA: age x genotype interaction; ADP, $F_{(1,5.66)} = 2.60$, $p = 0.026$; Fig 6D).

Lastly, reduced levels of the membrane phospholipid, phosphatidylcholine, were also observed in aging brain in inflammation (PERMANOVA: main effect: aging; phosphatidylcholine, $F_{(1,5.66)} = 6.77$, $p = 0.013$; (Fig 6D). In young mice but not aged mice, phosphatidylcholine concentrations positively correlated with glycerophosphatidylcholine concentrations (WT young $r^2 = 0.89$, $p = 0.04$; TSPO-KO young $r^2 = 0.93$, $p = 0.02$; WT old $r^2 = -0.79$, $p = 0.20$; TSPO-KO young $r^2 = 0.056$, $p = 0.92$). A significant interaction between TSPO-KO and aging was also identified for phosphatidylcholine (PERMANOVA: age x genotype interaction; phosphatidylcholine, $F_{(1,5.66)} = 3.63$, $p = 0.035$ (Fig 6D). Previous studies have demonstrated hippocampal phospholipid levels including phosphatidylcholine decline in aging. In addition to comprising the cell membrane, phosphatidylcholine is also a precursor for the major neurotransmitter acetylcholine(Chung et al., 1995), which is important in memory and depleted in AD (Giacobini et al., 2022; Liu et al., 2022). Interestingly, phosphatidylcholine has bene shown to inhibit LPS-induced inflammation and improve cognitive function (Tan et al., 2020), opening the possibility that age-related decline in hippocampal phosphatidylcholine may also play a role in inflammaging.

4 Conclusions

Broadly, our study indicates TSPO plays a protective role in brain aging, and that TSPO deletion exacerbates age-related transcriptional and metabolic changes in the inflamed hippocampus. This is of significance since we found TSPO levels in brain innate immune cells declined in aging. TSPO deletion aggravated key age-related synaptic and immune transcriptional signatures in the inflamed hippocampus, and these inflammaging signatures were mimicked by drugs that disrupt the cell cycle, cause DNA-damage and cell stress through the heat shock response. TSPO deletion also worsened age-related changes in brain metabolites, including depletion of the major inhibitory neurotransmitter GABA, and the anti-inflammatory TCA cycle metabolite, fumarate, providing a potential link between TSPO mitochondrial function and immune regulation. Importantly, we found an interaction between

TSPO-function and aging in the hippocampus. Aging resulted in a reversal of TSPO-KO transcriptional signatures following inflammatory insult. While we have previously shown that TSPO deletion dampens hippocampal inflammatory signatures in the young adult, we were surprised to discover that loss of TSPO drastically exacerbated inflammatory transcriptional responses in the aging hippocampus. This TSPO-aging interaction was linked to NF-kβ and interferon regulatory transcriptional networks. We verified TSPO-dependent modulation of NF-kβ activation in cultured microglia and macrophages. NF-kβ and interferons have been implicated in brain aging as well as the pathogenesis of AD. This TSPO-aging interaction is an important consideration in the interpretation of TSPO-targeted biomarker and therapeutic studies, as well as *in vitro* studies which cannot easily model brain aging.

CRediT authorship contribution statement

Kei Onn Lai: Conceptualization, Methodology, Investigation, Validation, Formal Analysis, Visualization, Writing – original draft. **Jia Hui Wong:** Methodology, Investigation, Validation, Formal Analysis, Visualization, Writing – revised draft. **Nevin Tham:** Methodology, Investigation, Validation, Formal Analysis, Visualization, Writing – original draft. **Lauren Fairley:** Methodology, Investigation, **Roshan Naik:** Methodology, Investigation. **Yulan Wang:** Methodology, Investigation, Validation, Formal Analysis, Visualization, Writing – review & editing. **Sarah R. Langley:** Methodology, Writing – review & editing. **Anna M. Barron:** Conceptualization, Formal Analysis, Visualization, Writing - original draft, Supervision, Funding acquisition.

Disclosure and competing interests: All authors declare nothing to disclose.

Data availability: Study data will be made available via https://researchdata.ntu.edu.sg/dataverse/neurobiologyaging repository.

5   References

Abreu, A. C., Navas, M. M., Fernández, C. P., Sánchez-Santed, F., & Fernández, I. (2021). NMR-Based Metabolomics Approach to Explore Brain Metabolic Changes Induced by Prenatal Exposure to Autism-Inducing Chemicals. *ACS Chem Biol*, *16*(4), 753-765. https://doi.org/10.1021/acschembio.1c00053

Álvarez-Rodríguez, L., López-Hoyos, M., Muñoz-Cacho, P., & Martínez-Taboada, V. M. (2012). Aging is associated with circulating cytokine dysregulation. *Cellular Immunology*, *273*(2), 124-132. https://doi.org/https://doi.org/10.1016/j.cellimm.2012.01.001

Ang, H. P., Makpol, S., Nasaruddin, M. L., Ahmad, N. S., Tan, J. K., Wan Zaidi, W. A., & Embong, H. (2023). Lipopolysaccharide-Induced Delirium-like Behaviour in a Rat Model of Chronic Cerebral Hypoperfusion Is Associated with Increased Indoleamine 2,3-Dioxygenase Expression and Endotoxin Tolerance. *Int J Mol Sci*, *24*(15). https://doi.org/10.3390/ijms241512248

Bader, S., Wolf, L., Milenkovic, V. M., Gruber, M., Nothdurfter, C., Rupprecht, R., & Wetzel, C. H. (2019). Differential effects of TSPO ligands on mitochondrial function in mouse microglia cells. *Psychoneuroendocrinology*, *106*, 65-76. https://doi.org/10.1016/j.psyneuen.2019.03.029

Bahaidrah, K. A., Alzahrani, N. A., Aldhahri, R. S., Mansouri, R. A., & Alghamdi, B. S. (2022). Effects of Different Lipopolysaccharide Doses on Short- and Long-Term Spatial Memory and Hippocampus Morphology in an Experimental Alzheimer's Disease Model. *Clinical and Translational Neuroscience*, *6*(3), 20. https://www.mdpi.com/2514-183X/6/3/20

Barron, A. M., Higuchi, M., Hattori, S., Kito, S., Suhara, T., & Ji, B. (2021). Regulation of Anxiety and Depression by Mitochondrial Translocator Protein-Mediated Steroidogenesis: the Role of Neurons. *Mol Neurobiol*, *58*(2), 550-563. https://doi.org/10.1007/s12035-020-02136-5

Barron, A. M., Ji, B., Kito, S., Suhara, T., & Higuchi, M. (2018). Steroidogenic abnormalities in translocator protein knockout mice and significance in the aging male. *Biochemical Journal*, *475*(1), 75-85. https://doi.org/10.1042/BCJ20170645

Benjaskulluecha, S., Boonmee, A., Pattarakankul, T., Wongprom, B., Klomsing, J., & Palaga, T. (2022). Screening of compounds to identify novel epigenetic regulatory factors that affect innate immune memory in macrophages. *Sci Rep*, *12*(1), 1912. https://doi.org/10.1038/s41598-022-05929-x

Bhat, M. F., Srdanović, S., Sundberg, L.-R., Einarsdóttir, H. K., Marjomäki, V., & Dekker, F. J. (2024). Impact of HDAC inhibitors on macrophage polarization to enhance innate immunity against infections. *Drug Discovery Today*, *29*(11), 104193. https://doi.org/https://doi.org/10.1016/j.drudis.2024.104193

Blevins, L. K., Crawford, R. B., Azzam, D. J., Guilarte, T. R., & Kaminski, N. E. (2021). Surface translocator protein 18 kDa (TSPO) localization on immune cells upon stimulation with LPS and in ART-treated HIV+ subjects. *Journal of Leukocyte Biology*, *110*(1), 123-140. https://doi.org/https://doi.org/10.1002/JLB.3A1219-729RR

Bradburn, S., Murgatroyd, C., & Ray, N. (2019). Neuroinflammation in mild cognitive impairment and Alzheimer's disease: A meta-analysis. *Ageing Res Rev*, *50*, 1-8. https://doi.org/10.1016/j.arr.2019.01.002

Brendel, M., Kleinberger, G., Probst, F., Jaworska, A., Overhoff, F., Blume, T., Albert, N. L., Carlsen, J., Lindner, S., Gildehaus, F. J., Ozmen, L., Suárez-Calvet, M., Bartenstein, P., Baumann, K., Ewers, M., Herms, J., Haass, C., & Rominger, A. (2017). Increase of TREM2 during Aging of an Alzheimer's Disease Mouse Model Is Paralleled by Microglial Activation and Amyloidosis [Original Research]. *Front Aging Neurosci*, *9*. https://doi.org/10.3389/fnagi.2017.00008

Brown, G. C., & Heneka, M. T. (2024). The endotoxin hypothesis of Alzheimer's disease. *Molecular Neurodegeneration*, *19*(1), 30. https://doi.org/10.1186/s13024-024-00722-y

Butler, T., Glodzik, L., Wang, X. H., Xi, K., Li, Y., Pan, H., Zhou, L., Chiang, G. C.-Y., Morim, S., Wickramasuriya, N., Tanzi, E., Maloney, T., Harvey, P., Mao, X., Razlighi, Q. R., Rusinek, H.,

Shungu, D. C., de Leon, M., Atwood, C. S., & Mozley, P. D. (2022). Positron Emission Tomography reveals age-associated hypothalamic microglial activation in women. *Sci Rep*, *12*(1), 13351. https://doi.org/10.1038/s41598-022-17315-8

Cagnin, A., Brooks, D. J., Kennedy, A. M., Gunn, R. N., Myers, R., Turkheimer, F. E., Jones, T., & Banati, R. B. (2001). In-vivo measurement of activated microglia in dementia. *Lancet*, *358*(9280), 461-467. https://doi.org/10.1016/s0140-6736(01)05625-2

Cammarota, M., & Boscia, F. (2023). Contribution of Oligodendrocytes, Microglia, and Astrocytes to Myelin Debris Uptake in an Explant Model of Inflammatory Demyelination in Rats. *Cells*, *12*(17). https://doi.org/10.3390/cells12172203

Chavoshinezhad, S., Safari, V., & Izadpanah, E. (2023). Intranasal interferon-beta as a promising alternative for the treatment of Alzheimer's disease. *Medical Hypotheses*, *170*, 110996. https://doi.org/https://doi.org/10.1016/j.mehy.2022.110996

Chung, S. Y., Moriyama, T., Uezu, E., Uezu, K., Hirata, R., Yohena, N., Masuda, Y., Kokubu, T., & Yamamoto, S. (1995). Administration of phosphatidylcholine increases brain acetylcholine concentration and improves memory in mice with dementia. *J Nutr*, *125*(6), 1484-1489. https://doi.org/10.1093/jn/125.6.1484

Cloarec, O., Dumas, M.-E., Craig, A., Barton, R. H., Trygg, J., Hudson, J., Blancher, C., Gauguier, D., Lindon, J. C., Holmes, E., & Nicholson, J. (2005). Statistical Total Correlation Spectroscopy: An Exploratory Approach for Latent Biomarker Identification from Metabolic 1H NMR Data Sets. *Anal Chem*, *77*(5), 1282-1289. https://doi.org/10.1021/ac048630x

Conde, J. R., & Streit, W. J. (2006). Microglia in the aging brain. *J Neuropathol Exp Neurol*, *65*(3), 199-203. https://doi.org/10.1097/01.jnen.0000202887.22082.63

Costa, J., Martins, S., Ferreira, P. A., Cardoso, A. M. S., Guedes, J. R., Peça, J., & Cardoso, A. L. (2021). The old guard: Age-related changes in microglia and their consequences. *Mechanisms of Ageing and Development*, *197*, 111512. https://doi.org/https://doi.org/10.1016/j.mad.2021.111512

Cribbs, D. H., Berchtold, N. C., Perreau, V., Coleman, P. D., Rogers, J., Tenner, A. J., & Cotman, C. W. (2012). Extensive innate immune gene activation accompanies brain aging, increasing vulnerability to cognitive decline and neurodegeneration: a microarray study. *J Neuroinflammation*, *9*(1), 179. https://doi.org/10.1186/1742-2094-9-179

Cullen, N. C., Mälarstig, A. n., Stomrud, E., Hansson, O., & Mattsson-Carlgren, N. (2021). Accelerated inflammatory aging in Alzheimer's disease and its relation to amyloid, tau, and cognition. *Sci Rep*, *11*(1), 1965. https://doi.org/10.1038/s41598-021-81705-7

Da Pozzo, E., Tremolanti, C., Costa, B., Giacomelli, C., Milenkovic, V. M., Bader, S., Wetzel, C. H., Rupprecht, R., Taliani, S., Da Settimo, F., & Martini, C. (2019). Microglial Pro-Inflammatory and Anti-Inflammatory Phenotypes Are Modulated by Translocator Protein Activation. *International Journal of Molecular Sciences*, *20*(18), 4467. https://www.mdpi.com/1422-0067/20/18/4467

Dai, Y., Rahmani, M., Dent, P., & Grant, S. (2005). Blockade of histone deacetylase inhibitor-induced RelA/p65 acetylation and NF-kappaB activation potentiates apoptosis in leukemia cells through a process mediated by oxidative damage, XIAP downregulation, and c-Jun N-terminal kinase 1 activation. *Mol Cell Biol*, *25*(13), 5429-5444. https://doi.org/10.1128/mcb.25.13.5429-5444.2005

Dani, M., Wood, M., Mizoguchi, R., Fan, Z., Walker, Z., Morgan, R., Hinz, R., Biju, M., Kuruvilla, T., Brooks, D. J., & Edison, P. (2018). Microglial activation correlates in vivo with both tau and amyloid in Alzheimer's disease. *Brain*, *141*(9), 2740-2754. https://doi.org/10.1093/brain/awy188

Debès, C., Papadakis, A., Grönke, S., Karalay, Ö., Tain, L. S., Mizi, A., Nakamura, S., Hahn, O., Weigelt, C., Josipovic, N., Zirkel, A., Brusius, I., Sofiadis, K., Lamprousi, M., Lu, Y.-X., Huang, W., Esmaillie, R., Kubacki, T., Späth, M. R., . . . Beyer, A. (2023). Ageing-associated changes in

transcriptional elongation influence longevity. *Nature*, *616*(7958), 814-821. https://doi.org/10.1038/s41586-023-05922-y

Desai, R., East, D. A., Hardy, L., Faccenda, D., Rigon, M., Crosby, J., Alvarez, M. S., Singh, A., Mainenti, M., Hussey, L. K., Bentham, R., Szabadkai, G., Zappulli, V., Dhoot, G. K., Romano, L. E., Xia, D., Coppens, I., Hamacher-Brady, A., Chapple, J. P., . . . Campanella, M. (2020). Mitochondria form contact sites with the nucleus to couple prosurvival retrograde response. *Science Advances*, *6*(51), eabc9955. https://doi.org/doi:10.1126/sciadv.abc9955

Duman, R. S., Sanacora, G., & Krystal, J. H. (2019). Altered Connectivity in Depression: GABA and Glutamate Neurotransmitter Deficits and Reversal by Novel Treatments. *Neuron*, *102*(1), 75-90. https://doi.org/10.1016/j.neuron.2019.03.013

Edison, P., Archer, H. A., Gerhard, A., Hinz, R., Pavese, N., Turkheimer, F. E., Hammers, A., Tai, Y. F., Fox, N., Kennedy, A., Rossor, M., & Brooks, D. J. (2008). Microglia, amyloid, and cognition in Alzheimer's disease: An [11C](R)PK11195-PET and [11C]PIB-PET study. *Neurobiol Dis*, *32*(3), 412-419. https://doi.org/10.1016/j.nbd.2008.08.001

Fairley, L. H., Lai, K. O., Wong, J. H., Chong, W. J., Vincent, A. S., D'Agostino, G., Wu, X., Naik, R. R., Jayaraman, A., Langley, S. R., Ruedl, C., & Barron, A. M. (2023). Mitochondrial control of microglial phagocytosis by the translocator protein and hexokinase 2 in Alzheimer's disease. *Proc Natl Acad Sci U S A*, *120*(8), e2209177120. https://doi.org/10.1073/pnas.2209177120

Fairley, L. H., Wong, J. H., & Barron, A. M. (2021). Mitochondrial Regulation of Microglial Immunometabolism in Alzheimer's Disease [Review]. *Frontiers in Immunology*, *12*. https://doi.org/10.3389/fimmu.2021.624538

Fan, J., & Papadopoulos, V. (2021). Mitochondrial TSPO Deficiency Triggers Retrograde Signaling in MA-10 Mouse Tumor Leydig Cells. *International Journal of Molecular Sciences*, *22*(1), 252. https://www.mdpi.com/1422-0067/22/1/252

Fan, Z., Aman, Y., Ahmed, I., Chetelat, G., Landeau, B., Ray Chaudhuri, K., Brooks, D. J., & Edison, P. (2015). Influence of microglial activation on neuronal function in Alzheimer's and Parkinson's disease dementia. *Alzheimers Dement*, *11*(6), 608-621.e607. https://doi.org/10.1016/j.jalz.2014.06.016

Finze, A., Biechele, G., Rauchmann, B. S., Franzmeier, N., Palleis, C., Katzdobler, S., Weidinger, E., Guersel, S., Schuster, S., Harris, S., Schmitt, J., Beyer, L., Gnörich, J., Lindner, S., Albert, N. L., Wetzel, C. H., Rupprecht, R., Rominger, A., Danek, A., . . . Brendel, M. (2023). Individual regional associations between Aβ-, tau- and neurodegeneration (ATN) with microglial activation in patients with primary and secondary tauopathies. *Mol Psychiatry*, *28*(10), 4438-4450. https://doi.org/10.1038/s41380-023-02188-8

Focke, C., Blume, T., Zott, B., Shi, Y., Deussing, M., Peters, F., Schmidt, C., Kleinberger, G., Lindner, S., Gildehaus, F.-J., Beyer, L., von Ungern-Sternberg, B., Bartenstein, P., Ozmen, L., Baumann, K., Dorostkar, M. M., Haass, C., Adelsberger, H., Herms, J., . . . Brendel, M. (2019). Early and Longitudinal Microglial Activation but Not Amyloid Accumulation Predicts Cognitive Outcome in PS2APP Mice. *Journal of Nuclear Medicine*, *60*(4), 548-554. https://doi.org/10.2967/jnumed.118.217703

Gatliff, J., East, D. A., Singh, A., Alvarez, M. S., Frison, M., Matic, I., Ferraina, C., Sampson, N., Turkheimer, F., & Campanella, M. (2017). A role for TSPO in mitochondrial Ca(2+) homeostasis and redox stress signaling. *Cell Death Dis*, *8*(6), e2896. https://doi.org/10.1038/cddis.2017.186

Gennady, K., Vladimir, S., Nikolay, B., Boris, S., Maxim, N. A., & Alexey, S. (2021). Fast gene set enrichment analysis. *bioRxiv*, 060012. https://doi.org/10.1101/060012

Giacobini, E., Cuello, A. C., & Fisher, A. (2022). Reimagining cholinergic therapy for Alzheimer's disease. *Brain*, *145*(7), 2250-2275. https://doi.org/10.1093/brain/awac096

Grimaldi, L. M. E., Zappalà, G., Iemolo, F., Castellano, A. E., Ruggieri, S., Bruno, G., & Paolillo, A. (2014). A pilot study on the use of interferon beta-1a in early Alzheimer's disease subjects. *J Neuroinflammation*, *11*(1), 30. https://doi.org/10.1186/1742-2094-11-30

Guilarte, T. R., Loth, M. K., & Guariglia, S. R. (2016). TSPO Finds NOX2 in Microglia for Redox Homeostasis. *Trends in Pharmacological Sciences*, *37*(5), 334-343. https://doi.org/https://doi.org/10.1016/j.tips.2016.02.008

Gulyás, B., Vas, A., Tóth, M., Takano, A., Varrone, A., Cselényi, Z., Schain, M., Mattsson, P., & Halldin, C. (2011). Age and disease related changes in the translocator protein (TSPO) system in the human brain: positron emission tomography measurements with [11C]vinpocetine. *Neuroimage*, *56*(3), 1111-1121. https://doi.org/10.1016/j.neuroimage.2011.02.020

Ham, S., & Lee, S.-J. V. (2020). Advances in transcriptome analysis of human brain aging. *Experimental & Molecular Medicine*, *52*(11), 1787-1797. https://doi.org/10.1038/s12276-020-00522-6

Hamelin, L., Lagarde, J., Dorothée, G., Leroy, C., Labit, M., Comley, R. A., de Souza, L. C., Corne, H., Dauphinot, L., Bertoux, M., Dubois, B., Gervais, P., Colliot, O., Potier, M. C., Bottlaender, M., & Sarazin, M. (2016). Early and protective microglial activation in Alzheimer's disease: a prospective study using 18F-DPA-714 PET imaging. *Brain*, *139*(Pt 4), 1252-1264. https://doi.org/10.1093/brain/aww017

Hao, Y., Stuart, T., Kowalski, M. H., Choudhary, S., Hoffman, P., Hartman, A., Srivastava, A., Molla, G., Madad, S., Fernandez-Granda, C., & Satija, R. (2024). Dictionary learning for integrative, multimodal and scalable single-cell analysis. *Nature Biotechnology*, *42*(2), 293-304. https://doi.org/10.1038/s41587-023-01767-y

Hayakawa, N., Kato, H., & Araki, T. (2007). Age-related changes of astorocytes, oligodendrocytes and microglia in the mouse hippocampal CA1 sector. *Mech Ageing Dev*, *128*(4), 311-316. https://doi.org/10.1016/j.mad.2007.01.005

Hefendehl, J. K., Neher, J. J., Sühs, R. B., Kohsaka, S., Skodras, A., & Jucker, M. (2014). Homeostatic and injury-induced microglia behavior in the aging brain. *Aging Cell*, *13*(1), 60-69. https://doi.org/10.1111/acel.12149

Heinz, S., Benner, C., Spann, N., Bertolino, E., Lin, Y. C., Laslo, P., Cheng, J. X., Murre, C., Singh, H., & Glass, C. K. (2010). Simple combinations of lineage-determining transcription factors prime cis-regulatory elements required for macrophage and B cell identities. *Mol Cell*, *38*(4), 576-589. https://doi.org/10.1016/j.molcel.2010.05.004

Hervé, M. R., Nicolè, F., & Lê Cao, K.-A. (2018). Multivariate Analysis of Multiple Datasets: a Practical Guide for Chemical Ecology. *Journal of Chemical Ecology*, *44*(3), 215-234. https://doi.org/10.1007/s10886-018-0932-6

Hirsch, J. D., Beyer, C. F., Malkowitz, L., Beer, B., & Blume, A. J. (1989). Mitochondrial benzodiazepine receptors mediate inhibition of mitochondrial respiratory control. *Molecular Pharmacology*, *35*(1), 157-163. https://doi.org/10.1016/S0026-895X(25)10080-1

Holtman, I. R., Raj, D. D., Miller, J. A., Schaafsma, W., Yin, Z., Brouwer, N., Wes, P. D., Möller, T., Orre, M., Kamphuis, W., Hol, E. M., Boddeke, E. W., & Eggen, B. J. (2015). Induction of a common microglia gene expression signature by aging and neurodegenerative conditions: a co-expression meta-analysis. *Acta Neuropathol Commun*, *3*, 31. https://doi.org/10.1186/s40478-015-0203-5

Horiguchi, Y., Ohta, N., Yamamoto, S., Koide, M., & Fujino, Y. (2019). Midazolam suppresses the lipopolysaccharide-stimulated immune responses of human macrophages via translocator protein signaling. *Int Immunopharmacol*, *66*, 373-382. https://doi.org/10.1016/j.intimp.2018.11.050

Hou, Y., Dan, X., Babbar, M., Wei, Y., Hasselbalch, S. G., Croteau, D. L., & Bohr, V. A. (2019). Ageing as a risk factor for neurodegenerative disease. *Nature Reviews Neurology*, *15*(10), 565-581. https://doi.org/10.1038/s41582-019-0244-7

Hussain, B., Fang, C., & Chang, J. (2021). Blood–Brain Barrier Breakdown: An Emerging Biomarker of Cognitive Impairment in Normal Aging and Dementia [Review]. *Frontiers in Neuroscience*, *15*. https://doi.org/10.3389/fnins.2021.688090

Janetka, J. W., & Ashwell, S. (2009). Checkpoint kinase inhibitors: a review of the patent literature. *Expert Opin Ther Pat*, *19*(2), 165-197. https://doi.org/10.1517/13543770802653622

Jullian, E., Russi, M., Turki, E., Bouvelot, M., Tixier, L., Middendorp, S., Martin, E., & Monnier, V. (2024). Glial overexpression of Tspo extends lifespan and protects against frataxin deficiency in Drosophila. *Biochimie*. https://doi.org/10.1016/j.biochi.2024.05.003

Kassambara, A. (2023). *rstatix: Pipe-Friendly Framework for Basic Statistical Tests*. https://cran.r-project.org/web/packages/rstatix/index.html

Katyal, S., Lee, Y., Nitiss, K. C., Downing, S. M., Li, Y., Shimada, M., Zhao, J., Russell, H. R., Petrini, J. H., Nitiss, J. L., & McKinnon, P. J. (2014). Aberrant topoisomerase-1 DNA lesions are pathogenic in neurodegenerative genome instability syndromes. *Nat Neurosci*, *17*(6), 813-821. https://doi.org/10.1038/nn.3715

Kealy, J., Murray, C., Griffin, E. W., Lopez-Rodriguez, A. B., Healy, D., Tortorelli, L. S., Lowry, J. P., Watne, L. O., & Cunningham, C. (2020). Acute Inflammation Alters Brain Energy Metabolism in Mice and Humans: Role in Suppressed Spontaneous Activity, Impaired Cognition, and Delirium. *J Neurosci*, *40*(29), 5681-5696. https://doi.org/10.1523/jneurosci.2876-19.2020

Kreisl, W. C., Lyoo, C. H., McGwier, M., Snow, J., Jenko, K. J., Kimura, N., Corona, W., Morse, C. L., Zoghbi, S. S., Pike, V. W., McMahon, F. J., Turner, R. S., & Innis, R. B. (2013). In vivo radioligand binding to translocator protein correlates with severity of Alzheimer's disease. *Brain*, *136*(Pt 7), 2228-2238. https://doi.org/10.1093/brain/awt145

Kumar, A., Muzik, O., Shandal, V., Chugani, D., Chakraborty, P., & Chugani, H. T. (2012). Evaluation of age-related changes in translocator protein (TSPO) in human brain using 11C-[R]-PK11195 PET. *J Neuroinflammation*, *9*(1), 232. https://doi.org/10.1186/1742-2094-9-232

Kurop, M. K., Huyen, C. M., Kelly, J. H., & Blagg, B. S. J. (2021). The heat shock response and small molecule regulators. *Eur J Med Chem*, *226*, 113846. https://doi.org/10.1016/j.ejmech.2021.113846

Langfelder, P., & Horvath, S. (2008). WGCNA: an R package for weighted correlation network analysis. *BMC Bioinformatics*, *9*, 559. https://doi.org/10.1186/1471-2105-9-559

Li, H., Zhu, W., Zhang, L., Lei, H., Wu, X., Guo, L., Chen, X., Wang, Y., & Tang, H. (2015). The metabolic responses to hepatitis B virus infection shed new light on pathogenesis and targets for treatment. *Sci Rep*, *5*(1), 8421. https://doi.org/10.1038/srep08421

Liang, N., Nho, K., Newman, J. W., Arnold, M., Huynh, K., Meikle, P. J., Borkowski, K., Kaddurah-Daouk, R., Kueider-Paisley, A., Doraiswamy, P. M., Blach, C., Moseley, A., Mahmoudiandehkhordi, S., Welsh-Balmer, K., Plassman, B., Saykin, A., Risacher, S., Kastenmüller, G., Han, X., . . . the Alzheimer's Disease Metabolomics, C. (2024). Peripheral inflammation is associated with brain atrophy and cognitive decline linked to mild cognitive impairment and Alzheimer's disease. *Sci Rep*, *14*(1), 17423. https://doi.org/10.1038/s41598-024-67177-5

Lin, K., Li, L., Dai, Y., Wang, H., Teng, S., Bao, X., Lu, Z. J., & Wang, D. (2020). A comprehensive evaluation of connectivity methods for L1000 data. *Briefings in Bioinformatics*, *21*(6), 2194-2205. https://doi.org/10.1093/bib/bbz129

Liu, G. J., Middleton, R. J., Kam, W. W., Chin, D. Y., Hatty, C. R., Chan, R. H., & Banati, R. B. (2017). Functional gains in energy and cell metabolism after TSPO gene insertion. *Cell Cycle*, *16*(5), 436-447. https://doi.org/10.1080/15384101.2017.1281477

Liu, W., Li, J., Yang, M., Ke, X., Dai, Y., Lin, H., Wang, S., Chen, L., & Tao, J. (2022). Chemical genetic activation of the cholinergic basal forebrain hippocampal circuit rescues memory loss in Alzheimer's disease. *Alzheimer's Research & Therapy*, *14*(1), 53. https://doi.org/10.1186/s13195-022-00994-w

Lopes, K. d. P., Snijders, G. J. L., Humphrey, J., Allan, A., Sneeboer, M. A. M., Navarro, E., Schilder, B. M., Vialle, R. A., Parks, M., Missall, R., van Zuiden, W., Gigase, F. A. J., Kübler, R., van Berlekom, A. B., Hicks, E. M., Böttcher, C., Priller, J., Kahn, R. S., de Witte, L. D., & Raj, T. (2022). Genetic analysis of the human microglial transcriptome across brain regions, aging

and disease pathologies. *Nature Genetics*, *54*(1), 4-17. https://doi.org/10.1038/s41588-021-00976-y

López-Otín, C., Blasco, M. A., Partridge, L., Serrano, M., & Kroemer, G. (2013). The hallmarks of aging. *Cell*, *153*(6), 1194-1217. https://doi.org/10.1016/j.cell.2013.05.039

Loth, M. K., Guariglia, S. R., Re, D. B., Perez, J., de Paiva, V. N., Dziedzic, J. L., Chambers, J. W., Azzam, D. J., & Guilarte, T. R. (2020). A Novel Interaction of Translocator Protein 18 kDa (TSPO) with NADPH Oxidase in Microglia. *Mol Neurobiol*, *57*(11), 4467-4487. https://doi.org/10.1007/s12035-020-02042-w

Love, M. I., Huber, W., & Anders, S. (2014). Moderated estimation of fold change and dispersion for RNA-seq data with DESeq2. *Genome Biology*, *15*(12), 550. https://doi.org/10.1186/s13059-014-0550-8

MacAskill, M. G., Stadulyte, A., Williams, L., Morgan, T. E. F., Sloan, N. L., Alcaide-Corral, C. J., Walton, T., Wimberley, C., McKenzie, C.-A., Spath, N., Mungall, W., BouHaidar, R., Dweck, M. R., Gray, G. A., Newby, D. E., Lucatelli, C., Sutherland, A., Pimlott, S. L., & Tavares, A. A. S. (2021). Quantification of Macrophage-Driven Inflammation During Myocardial Infarction with ^{18}F-LW223, a Novel TSPO Radiotracer with Binding Independent of the rs6971 Human Polymorphism. *Journal of Nuclear Medicine*, *62*(4), 536-544. https://doi.org/10.2967/jnumed.120.243600

Milenkovic, V. M., Slim, D., Bader, S., Koch, V., Heinl, E. S., Alvarez-Carbonell, D., Nothdurfter, C., Rupprecht, R., & Wetzel, C. H. (2019). CRISPR-Cas9 Mediated TSPO Gene Knockout alters Respiration and Cellular Metabolism in Human Primary Microglia Cells. *Int J Mol Sci*, *20*(13). https://doi.org/10.3390/ijms20133359

Miljković, D., Blaževski, J., Petković, F., Djedović, N., Momčilović, M., Stanisavljević, S., Jevtić, B., Mostarica Stojković, M., & Spasojević, I. (2015). A Comparative Analysis of Multiple Sclerosis–Relevant Anti-Inflammatory Properties of Ethyl Pyruvate and Dimethyl Fumarate. *The Journal of Immunology*, *194*(6), 2493-2503. https://doi.org/10.4049/jimmunol.1402302

Miller, K. R., & Streit, W. J. (2007). The effects of aging, injury and disease on microglial function: a case for cellular senescence. *Neuron Glia Biol*, *3*(3), 245-253. https://doi.org/10.1017/s1740925x08000136

Min, K. Y., Lee, M. B., Hong, S. H., Lee, D., Jo, M. G., Lee, J. E., Choi, M. Y., You, J. S., Kim, Y. M., Park, Y. M., Kim, H. S., & Choi, W. S. (2021). Entinostat, a histone deacetylase inhibitor, increases the population of IL-10(+) regulatory B cells to suppress contact hypersensitivity. *BMB Rep*, *54*(10), 534-539. https://doi.org/10.5483/BMBRep.2021.54.10.092

Mudò, G., Frinchi, M., Nuzzo, D., Scaduto, P., Plescia, F., Massenti, M. F., Di Carlo, M., Cannizzaro, C., Cassata, G., Cicero, L., Ruscica, M., Belluardo, N., & Grimaldi, L. M. (2019). Anti-inflammatory and cognitive effects of interferon-β1a (IFNβ1a) in a rat model of Alzheimer's disease. *J Neuroinflammation*, *16*(1), 44. https://doi.org/10.1186/s12974-019-1417-4

Newman, A. M., Steen, C. B., Liu, C. L., Gentles, A. J., Chaudhuri, A. A., Scherer, F., Khodadoust, M. S., Esfahani, M. S., Luca, B. A., Steiner, D., Diehn, M., & Alizadeh, A. A. (2019). Determining cell type abundance and expression from bulk tissues with digital cytometry. *Nature Biotechnology*, *37*(7), 773-782. https://doi.org/10.1038/s41587-019-0114-2

Nishiguchi, T., Yamanishi, K., Gorantla, N., Shimura, A., Seki, T., Ishii, T., Aoyama, B., Malicoat, J. R., Phuong, N. J., Dye, N. J., Yamanashi, T., Iwata, M., & Shinozaki, G. (2024). Lipopolysaccharide-Induced Delirium-Like Behavior and Microglial Activation in Mice Correlate With Bispectral Electroencephalography. *The Journals of Gerontology: Series A*, *79*(12), glae261. https://doi.org/10.1093/gerona/glae261

Novoa, C., Salazar, P., Cisternas, P., Gherardelli, C., Vera-Salazar, R., Zolezzi, J. M., & Inestrosa, N. C. (2022). Inflammation context in Alzheimer's disease, a relationship intricate to define. *Biological Research*, *55*(1), 39. https://doi.org/10.1186/s40659-022-00404-3

Nutma, E., Ceyzériat, K., Amor, S., Tsartsalis, S., Millet, P., Owen, D. R., Papadopoulos, V., & Tournier, B. B. (2021). Cellular sources of TSPO expression in healthy and diseased brain. *Eur J Nucl Med Mol Imaging*, *49*(1), 146-163. https://doi.org/10.1007/s00259-020-05166-2

Nutma, E., Fancy, N., Weinert, M., Tsartsalis, S., Marzin, M. C., Muirhead, R. C. J., Falk, I., Breur, M., de Bruin, J., Hollaus, D., Pieterman, R., Anink, J., Story, D., Chandran, S., Tang, J., Trolese, M. C., Saito, T., Saido, T. C., Wiltshire, K. H., . . . Owen, D. R. (2023). Translocator protein is a marker of activated microglia in rodent models but not human neurodegenerative diseases. *Nature Communications*, *14*(1), 5247. https://doi.org/10.1038/s41467-023-40937-z

Olah, M., Patrick, E., Villani, A.-C., Xu, J., White, C. C., Ryan, K. J., Piehowski, P., Kapasi, A., Nejad, P., Cimpean, M., Connor, S., Yung, C. J., Frangieh, M., McHenry, A., Elyaman, W., Petyuk, V., Schneider, J. A., Bennett, D. A., De Jager, P. L., & Bradshaw, E. M. (2018). A transcriptomic atlas of aged human microglia. *Nature Communications*, *9*(1), 539. https://doi.org/10.1038/s41467-018-02926-5

Parbo, P., Ismail, R., Hansen, K. V., Amidi, A., Mårup, F. H., Gottrup, H., Brændgaard, H., Eriksson, B. O., Eskildsen, S. F., Lund, T. E., Tietze, A., Edison, P., Pavese, N., Stokholm, M. G., Borghammer, P., Hinz, R., Aanerud, J., & Brooks, D. J. (2017). Brain inflammation accompanies amyloid in the majority of mild cognitive impairment cases due to Alzheimer's disease. *Brain*, *140*(7), 2002-2011. https://doi.org/10.1093/brain/awx120

Parry, D., Guzi, T., Shanahan, F., Davis, N., Prabhavalkar, D., Wiswell, D., Seghezzi, W., Paruch, K., Dwyer, M. P., Doll, R., Nomeir, A., Windsor, W., Fischmann, T., Wang, Y., Oft, M., Chen, T., Kirschmeier, P., & Lees, E. M. (2010). Dinaciclib (SCH 727965), a novel and potent cyclin-dependent kinase inhibitor. *Mol Cancer Ther*, *9*(8), 2344-2353. https://doi.org/10.1158/1535-7163.Mct-10-0324

Pascoal, T. A., Benedet, A. L., Ashton, N. J., Kang, M. S., Therriault, J., Chamoun, M., Savard, M., Lussier, F. Z., Tissot, C., Karikari, T. K., Ottoy, J., Mathotaarachchi, S., Stevenson, J., Massarweh, G., Schöll, M., de Leon, M. J., Soucy, J. P., Edison, P., Blennow, K., . . . Rosa-Neto, P. (2021). Microglial activation and tau propagate jointly across Braak stages. *Nat Med*, *27*(9), 1592-1599. https://doi.org/10.1038/s41591-021-01456-w

Paul, S., Gallagher, E., Liow, J. S., Mabins, S., Henry, K., Zoghbi, S. S., Gunn, R. N., Kreisl, W. C., Richards, E. M., Zanotti-Fregonara, P., Morse, C. L., Hong, J., Kowalski, A., Pike, V. W., Innis, R. B., & Fujita, M. (2019). Building a database for brain 18 kDa translocator protein imaged using [(11)C]PBR28 in healthy subjects. *J Cereb Blood Flow Metab*, *39*(6), 1138-1147. https://doi.org/10.1177/0271678x18771250

Perez-Dominguez, M., Ávila-Muñoz, E., Domínguez-Rivas, E., & Zepeda, A. (2019). The detrimental effects of lipopolysaccharide-induced neuroinflammation on adult hippocampal neurogenesis depend on the duration of the pro-inflammatory response. *Neural Regen Res*, *14*(5), 817-825. https://doi.org/10.4103/1673-5374.249229

Pradhan, A. K., Neumüller, T., Klug, C., Fuchs, S., Schlegel, M., Ballmann, M., Tartler, K. J., Pianos, A., Garcia, M. S., Liere, P., Schumacher, M., Kreuzer, M., Rupprecht, R., & Rammes, G. (2023). Chronic administration of XBD173 ameliorates cognitive deficits and neuropathology via 18 kDa translocator protein (TSPO) in a mouse model of Alzheimer's disease. *Translational Psychiatry*, *13*(1), 332. https://doi.org/10.1038/s41398-023-02630-z

Repalli, J. (2014). Translocator protein (TSPO) role in aging and Alzheimer's disease. *Curr Aging Sci*, *7*(3), 168-175. https://doi.org/10.2174/1874609808666141210103146

Robinson, M. D., McCarthy, D. J., & Smyth, G. K. (2010). edgeR: a Bioconductor package for differential expression analysis of digital gene expression data. *Bioinformatics*, *26*(1), 139-140. https://doi.org/10.1093/bioinformatics/btp616

Rohart, F., Gautier, B., Singh, A., & Lê Cao, K.-A. (2017). mixOmics: An R package for 'omics feature selection and multiple data integration. *PLOS Computational Biology*, *13*(11), e1005752. https://doi.org/10.1371/journal.pcbi.1005752

Ryu, Y., Kee, H. J., Sun, S., Seok, Y. M., Choi, S. Y., Kim, G. R., Kee, S.-J., Pflieger, M., Kurz, T., Kim, H.-S., & Jeong, M. H. (2019). Class I histone deacetylase inhibitor MS-275 attenuates vasoconstriction and inflammation in angiotensin II-induced hypertension. *PLoS One*, *14*(3), e0213186. https://doi.org/10.1371/journal.pone.0213186

Salminen, A., Huuskonen, J., Ojala, J., Kauppinen, A., Kaarniranta, K., & Suuronen, T. (2008). Activation of innate immunity system during aging: NF-kB signaling is the molecular culprit of inflamm-aging. *Ageing Research Reviews*, *7*(2), 83-105. https://doi.org/https://doi.org/10.1016/j.arr.2007.09.002

Salminen, A., Kauppinen, A., & Kaarniranta, K. (2012). Emerging role of NF-κB signaling in the induction of senescence-associated secretory phenotype (SASP). *Cellular Signalling*, *24*(4), 835-845. https://doi.org/https://doi.org/10.1016/j.cellsig.2011.12.006

Sandiego, C. M., Gallezot, J. D., Pittman, B., Nabulsi, N., Lim, K., Lin, S. F., Matuskey, D., Lee, J. Y., O'Connor, K. C., Huang, Y., Carson, R. E., Hannestad, J., & Cosgrove, K. P. (2015). Imaging robust microglial activation after lipopolysaccharide administration in humans with PET. *Proc Natl Acad Sci U S A*, *112*(40), 12468-12473. https://doi.org/10.1073/pnas.1511003112

Schaum, N., Lehallier, B., Hahn, O., Pálovics, R., Hosseinzadeh, S., Lee, S. E., Sit, R., Lee, D. P., Losada, P. M., Zardeneta, M. E., Fehlmann, T., Webber, J. T., McGeever, A., Calcuttawala, K., Zhang, H., Berdnik, D., Mathur, V., Tan, W., Zee, A., . . . The Tabula Muris, C. (2020). Ageing hallmarks exhibit organ-specific temporal signatures. *Nature*, *583*(7817), 596-602. https://doi.org/10.1038/s41586-020-2499-y

Schuitemaker, A., van der Doef, T. F., Boellaard, R., van der Flier, W. M., Yaqub, M., Windhorst, A. D., Barkhof, F., Jonker, C., Kloet, R. W., Lammertsma, A. A., Scheltens, P., & van Berckel, B. N. (2012). Microglial activation in healthy aging. *Neurobiol Aging*, *33*(6), 1067-1072. https://doi.org/10.1016/j.neurobiolaging.2010.09.016

Searle, S. R., Speed, F. M., & Milliken, G. A. (1980). Population Marginal Means in the Linear Model: An Alternative to Least Squares Means. *The American Statistician*, *34*(4), 216-221. https://doi.org/10.1080/00031305.1980.10483031

Shah, S., Sinharay, S., Patel, R., Solomon, J., Lee, J. H., Schreiber-Stainthorp, W., Basuli, F., Zhang, X., Hagen, K. R., Reeder, R., Wakim, P., Huzella, L. M., Maric, D., Johnson, R. F., & Hammoud, D. A. (2022). PET imaging of TSPO expression in immune cells can assess organ-level pathophysiology in high-consequence viral infections. *Proceedings of the National Academy of Sciences*, *119*(15), e2110846119. https://doi.org/10.1073/pnas.2110846119

Sharaf, A., Krieglstein, K., & Spittau, B. (2013). Distribution of microglia in the postnatal murine nigrostriatal system. *Cell Tissue Res*, *351*(3), 373-382. https://doi.org/10.1007/s00441-012-1537-y

Shen, L. (2023). *GeneOverlap: Test and visualize gene overlaps*. https://bioconductor.org/packages/GeneOverlap.

Sheng, J., Ruedl, C., & Karjalainen, K. (2019). Brain microglia is maintained and regenerated from a specialized cellular subset. EUROPEAN JOURNAL OF IMMUNOLOGY,

Shimoyama, S., Furukawa, T., Ogata, Y., Nikaido, Y., Koga, K., Sakamoto, Y., Ueno, S., & Nakamura, K. (2019). Lipopolysaccharide induces mouse translocator protein (18 kDa) expression via the AP-1 complex in the microglial cell line, BV-2. *PLoS One*, *14*(9), e0222861. https://doi.org/10.1371/journal.pone.0222861

Sidiropoulos, D. N., Rafie, C. I., Jang, J. K., Castanon, S., Baugh, A. G., Gonzalez, E., Christmas, B. J., Narumi, V. H., Davis-Marcisak, E. F., Sharma, G., Bigelow, E., Vaghasia, A., Gupta, A., Skaist, A., Considine, M., Wheelan, S. J., Ganesan, S. K., Yu, M., Yegnasubramanian, S., . . . Roussos Torres, E. T. (2022). Entinostat Decreases Immune Suppression to Promote Antitumor Responses in a HER2+ Breast Tumor Microenvironment. *Cancer Immunol Res*, *10*(5), 656-669. https://doi.org/10.1158/2326-6066.Cir-21-0170

Sierra, A., Gottfried-Blackmore, A. C., McEwen, B. S., & Bulloch, K. (2007). Microglia derived from aging mice exhibit an altered inflammatory profile. *Glia*, *55*(4), 412-424. https://doi.org/https://doi.org/10.1002/glia.20468

Silvin, A., Uderhardt, S., Piot, C., Da Mesquita, S., Yang, K., Geirsdottir, L., Mulder, K., Eyal, D., Liu, Z., Bridlance, C., Thion, M. S., Zhang, X. M., Kong, W. T., Deloger, M., Fontes, V., Weiner, A., Ee, R., Dress, R., Hang, J. W., . . . Ginhoux, F. (2022). Dual ontogeny of disease-associated microglia and disease inflammatory macrophages in aging and neurodegeneration. *Immunity*, *55*(8), 1448-1465.e1446. https://doi.org/10.1016/j.immuni.2022.07.004

Smith, G., Rani, A., Kumar, A., Barter, J., & Foster, T. C. (2020). Hippocampal Subregion Transcriptomic Profiles Reflect Strategy Selection during Cognitive Aging. *J Neurosci*, *40*(25), 4888-4899. https://doi.org/10.1523/jneurosci.2944-19.2020

Songkiatisak, P., Rahman, S. M. T., Aqdas, M., & Sung, M.-H. (2022). NF-κB, a culprit of both inflamm-ageing and declining immunity? *Immunity & Ageing*, *19*(1), 20. https://doi.org/10.1186/s12979-022-00277-w

Stanfield, B. A., Purves, T., Palmer, S., Sullenger, B., Welty-Wolf, K., Haines, K., Agarwal, S., & Kasotakis, G. (2021). IL-10 and class 1 histone deacetylases act synergistically and independently on the secretion of proinflammatory mediators in alveolar macrophages. *PLoS One*, *16*(1), e0245169. https://doi.org/10.1371/journal.pone.0245169

Stephens, M. (2017). False discovery rates: a new deal. *Biostatistics*, *18*(2), 275-294. https://doi.org/10.1093/biostatistics/kxw041

Streit, W. J., Miller, K. R., Lopes, K. O., & Njie, E. (2008). Microglial degeneration in the aging brain--bad news for neurons? *Front Biosci*, *13*, 3423-3438. https://doi.org/10.2741/2937

Stuesse, S. L., Cruce, W. L., Lovell, J. A., McBurney, D. L., & Crisp, T. (2000). Microglial proliferation in the spinal cord of aged rats with a sciatic nerve injury. *Neurosci Lett*, *287*(2), 121-124. https://doi.org/10.1016/s0304-3940(00)01142-3

Subramanian, A., Narayan, R., Corsello, S. M., Peck, D. D., Natoli, T. E., Lu, X., Gould, J., Davis, J. F., Tubelli, A. A., Asiedu, J. K., Lahr, D. L., Hirschman, J. E., Liu, Z., Donahue, M., Julian, B., Khan, M., Wadden, D., Smith, I. C., Lam, D., . . . Golub, T. R. (2017). A Next Generation Connectivity Map: L1000 Platform and the First 1,000,000 Profiles. *Cell*, *171*(6), 1437-1452.e1417. https://doi.org/10.1016/j.cell.2017.10.049

Sultan, Z. W., Jaeckel, E. R., Krause, B. M., Grady, S. M., Murphy, C. A., Sanders, R. D., & Banks, M. I. (2021). Electrophysiological signatures of acute systemic lipopolysaccharide-induced inflammation: potential implications for delirium science. *British Journal of Anaesthesia*, *126*(5), 996-1008. https://doi.org/https://doi.org/10.1016/j.bja.2020.12.040

Sun, E., Motolani, A., Campos, L., & Lu, T. (2022). The Pivotal Role of NF-kB in the Pathogenesis and Therapeutics of Alzheimer's Disease. *Int J Mol Sci*, *23*(16). https://doi.org/10.3390/ijms23168972

Suridjan, I., Rusjan, P. M., Voineskos, A. N., Selvanathan, T., Setiawan, E., Strafella, A. P., Wilson, A. A., Meyer, J. H., Houle, S., & Mizrahi, R. (2014). Neuroinflammation in healthy aging: a PET study using a novel Translocator Protein 18kDa (TSPO) radioligand, [(18)F]-FEPPA. *Neuroimage*, *84*, 868-875. https://doi.org/10.1016/j.neuroimage.2013.09.021

Szklarczyk, D., Gable, A. L., Nastou, K. C., Lyon, D., Kirsch, R., Pyysalo, S., Doncheva, N. T., Legeay, M., Fang, T., Bork, P., Jensen, L. J., & von Mering, C. (2021). The STRING database in 2021: customizable protein–protein networks, and functional characterization of user-uploaded gene/measurement sets. *Nucleic Acids Res*, *49*(D1), D605-D612. https://doi.org/10.1093/nar/gkaa1074

Tan, W., Zhang, Q., Dong, Z., Yan, Y., Fu, Y., Liu, X., Zhao, B., & Duan, X. (2020). Phosphatidylcholine Ameliorates LPS-Induced Systemic Inflammation and Cognitive Impairments via Mediating the Gut–Brain Axis Balance. *Journal of Agricultural and Food Chemistry*, *68*(50), 14884-14895. https://doi.org/10.1021/acs.jafc.0c06383

Taylor, J. M., Allen, A. M., & Graham, A. (2014). Targeting mitochondrial 18 kDa translocator protein (TSPO) regulates macrophage cholesterol efflux and lipid phenotype. *Clin Sci (Lond)*, *127*(10), 603-613. https://doi.org/10.1042/cs20140047

Tham, N., & Langley, S. R. (2022). Evaluating the robustness of connectivity methods to noise for in silico drug repurposing studies [Original Research]. *Frontiers in Systems Biology*, *2*. https://doi.org/10.3389/fsysb.2022.1050730

Thomas, A. L., Lehn, M. A., Janssen, E. M., Hildeman, D. A., & Chougnet, C. A. (2022). Naturally-aged microglia exhibit phagocytic dysfunction accompanied by gene expression changes reflective of underlying neurologic disease. *Sci Rep*, *12*(1), 19471. https://doi.org/10.1038/s41598-022-21920-y

Tommasini, D., & Fogel, B. L. (2023). multiWGCNA: an R package for deep mining gene co-expression networks in multi-trait expression data. *BMC Bioinformatics*, *24*(1), 115. https://doi.org/10.1186/s12859-023-05233-z

Tremblay, M., Zettel, M. L., Ison, J. R., Allen, P. D., & Majewska, A. K. (2012). Effects of aging and sensory loss on glial cells in mouse visual and auditory cortices. *Glia*, *60*(4), 541-558. https://doi.org/10.1002/glia.22287

Valero, J., Mastrella, G., Neiva, I., Sánchez, S., & Malva, J. O. (2014). Long-term effects of an acute and systemic administration of LPS on adult neurogenesis and spatial memory [Original Research]. *Frontiers in Neuroscience*, *8*. https://doi.org/10.3389/fnins.2014.00083

VanGuilder, H. D., Bixler, G. V., Brucklacher, R. M., Farley, J. A., Yan, H., Warrington, J. P., Sonntag, W. E., & Freeman, W. M. (2011). Concurrent hippocampal induction of MHC II pathway components and glial activation with advanced aging is not correlated with cognitive impairment. *J Neuroinflammation*, *8*(1), 138. https://doi.org/10.1186/1742-2094-8-138

Varrone, A., Oikonen, V., Forsberg, A., Joutsa, J., Takano, A., Solin, O., Haaparanta-Solin, M., Nag, S., Nakao, R., Al-Tawil, N., Wells, L. A., Rabiner, E. A., Valencia, R., Schultze-Mosgau, M., Thiele, A., Vollmer, S., Dyrks, T., Lehmann, L., Heinrich, T., . . . Rinne, J. O. (2015). Positron emission tomography imaging of the 18-kDa translocator protein (TSPO) with [18F]FEMPA in Alzheimer's disease patients and control subjects. *Eur J Nucl Med Mol Imaging*, *42*(3), 438-446. https://doi.org/10.1007/s00259-014-2955-8

Versijpt, J. J., Dumont, F., Van Laere, K. J., Decoo, D., Santens, P., Audenaert, K., Achten, E., Slegers, G., Dierckx, R. A., & Korf, J. (2003). Assessment of neuroinflammation and microglial activation in Alzheimer's disease with radiolabelled PK11195 and single photon emission computed tomography. A pilot study. *Eur Neurol*, *50*(1), 39-47. https://doi.org/10.1159/000070857

Victorio, C. B. L., Ganasarajah, A., Novera, W., Ong, J., Msallam, R., & Chacko, A.-M. (2024). Translocator protein (TSPO) is a biomarker of Zika virus (ZIKV) infection-associated neuroinflammation. *Emerging Microbes & Infections*, *13*(1), 2348528. https://doi.org/10.1080/22221751.2024.2348528

Wang, Y., Tang, H., Holmes, E., Lindon, J. C., Turini, M. E., Sprenger, N., Bergonzelli, G., Fay, L. B., Kochhar, S., & Nicholson, J. K. (2005). Biochemical Characterization of Rat Intestine Development Using High-Resolution Magic-Angle-Spinning 1H NMR Spectroscopy and Multivariate Data Analysis. *Journal of Proteome Research*, *4*(4), 1324-1329. https://doi.org/10.1021/pr050032r

Webster, K. R., & Kimball, S. D. (2000). Novel drugs targeting the cell cycle. *Emerging Drugs*, *5*(1), 45-59. https://doi.org/10.1517/14728214.5.1.45

Wickham, H. (2016). *ggplot2: Elegant Graphics for Data Analysis.* Springer-Verlag New York. https://ggplot2.tidyverse.org.

Wimberley, C., Lavisse, S., Hillmer, A., Hinz, R., Turkheimer, F., & Zanotti-Fregonara, P. (2021). Kinetic modeling and parameter estimation of TSPO PET imaging in the human brain. *Eur J Nucl Med Mol Imaging*, *49*(1), 246-256. https://doi.org/10.1007/s00259-021-05248-9

Wright, P., Veronese, M., Mazibuko, N., Turkheimer, F. E., Rabiner, E. A., Ballard, C. G., Williams, S. C. R., Hari Narayanan, A. K., Osrah, B., Williams, R., Marques, T. R., Howes, O. D., Roncaroli, F., & O'Sullivan, M. J. (2020). Patterns of Mitochondrial TSPO Binding in Cerebral Small Vessel Disease: An in vivo PET Study With Neuropathological Comparison. *Front Neurol*, *11*, 541377. https://doi.org/10.3389/fneur.2020.541377

Wu, X., Saito, T., Saido, T. C., Barron, A. M., & Ruedl, C. (2021). Microglia and CD206+ border-associated mouse macrophages maintain their embryonic origin during Alzheimer's disease. *Elife*, *10*, e71879. https://doi.org/10.7554/eLife.71879

Xia, J., Psychogios, N., Young, N., & Wishart, D. S. (2009). MetaboAnalyst: a web server for metabolomic data analysis and interpretation. *Nucleic Acids Res*, *37*(Web Server issue), W652-660. https://doi.org/10.1093/nar/gkp356

Yasuno, F., Kosaka, J., Ota, M., Higuchi, M., Ito, H., Fujimura, Y., Nozaki, S., Takahashi, S., Mizukami, K., Asada, T., & Suhara, T. (2012). Increased binding of peripheral benzodiazepine receptor in mild cognitive impairment-dementia converters measured by positron emission tomography with [^{11}C]DAA1106. *Psychiatry Res*, *203*(1), 67-74. https://doi.org/10.1016/j.pscychresns.2011.08.013

Ye, S. M., & Johnson, R. W. (1999). Increased interleukin-6 expression by microglia from brain of aged mice. *J Neuroimmunol*, *93*(1-2), 139-148. https://doi.org/10.1016/s0165-5728(98)00217-3

Yokokura, M., Terada, T., Bunai, T., Nakaizumi, K., Takebayashi, K., Iwata, Y., Yoshikawa, E., Futatsubashi, M., Suzuki, K., Mori, N., & Ouchi, Y. (2017). Depiction of microglial activation in aging and dementia: Positron emission tomography with [(11)C]DPA713 versus [(11)C](R)PK11195. *J Cereb Blood Flow Metab*, *37*(3), 877-889. https://doi.org/10.1177/0271678x16646788

Yu, L. L., Yu, H. G., Yu, J. P., Luo, H. S., Xu, X. M., & Li, J. H. (2004). Nuclear factor-kappaB p65 (RelA) transcription factor is constitutively activated in human colorectal carcinoma tissue. *World J Gastroenterol*, *10*(22), 3255-3260. https://doi.org/10.3748/wjg.v10.i22.3255

Zeisel, A., Muñoz-Manchado, A. B., Codeluppi, S., Lönnerberg, P., La Manno, G., Juréus, A., Marques, S., Munguba, H., He, L., Betsholtz, C., Rolny, C., Castelo-Branco, G., Hjerling-Leffler, J., & Linnarsson, S. (2015). Cell types in the mouse cortex and hippocampus revealed by single-cell RNA-seq. *Science*, *347*(6226), 1138-1142. https://doi.org/10.1126/science.aaa1934

Zhang, G., Lu, J., Zheng, J., Mei, S., Li, H., Zhang, X., Ping, A., Gao, S., Fang, Y., & Yu, J. (2024). Spi1 regulates the microglial/macrophage inflammatory response via the PI3K/AKT/mTOR signaling pathway after intracerebral hemorrhage. *Neural Regen Res*, *19*(1), 161-170. https://doi.org/10.4103/1673-5374.375343

Zhang, H., Wang, H., Gao, F., Yang, J., Xu, Y., Fu, Y., Cai, M., Zhang, X., Yang, Q., Tong, K., Hu, Y., Chen, H., Ma, C., He, W., & Zhang, J. (2021). TSPO deficiency accelerates amyloid pathology and neuroinflammation by impairing microglial phagocytosis. *Neurobiology of Aging*, *106*, 292-303. https://doi.org/https://doi.org/10.1016/j.neurobiolaging.2021.06.020

Zhang, J., Ma, L., Wan, X., Shan, J., Qu, Y., & Hashimoto, K. (2021). (R)-Ketamine attenuates LPS-induced endotoxin-derived delirium through inhibition of neuroinflammation. *Psychopharmacology (Berl)*, *238*(10), 2743-2753. https://doi.org/10.1007/s00213-021-05889-6

Zhang, S. D., & Gant, T. W. (2008). A simple and robust method for connecting small-molecule drugs using gene-expression signatures. *BMC Bioinformatics*, *9*, 258. https://doi.org/10.1186/1471-2105-9-258

Zhang, X., Liu, Y., Hong, X., Li, X., Meshul, C. K., Moore, C., Yang, Y., Han, Y., Li, W.-G., Qi, X., Lou, H., Duan, S., Xu, T.-L., & Tong, X. (2021). NG2 glia-derived GABA release tunes inhibitory synapses and contributes to stress-induced anxiety. *Nature Communications*, *12*(1), 5740. https://doi.org/10.1038/s41467-021-25956-y

Zhao, Y. Y., Yu, J. Z., Li, Q. Y., Ma, C. G., Lu, C. Z., & Xiao, B. G. (2011). TSPO-specific ligand vinpocetine exerts a neuroprotective effect by suppressing microglial inflammation. *Neuron Glia Biol*, *7*(2-4), 187-197. https://doi.org/10.1017/s1740925x12000129

Zhou, G., Soufan, O., Ewald, J., Hancock, R. E. W., Basu, N., & Xia, J. (2019). NetworkAnalyst 3.0: a visual analytics platform for comprehensive gene expression profiling and meta-analysis. *Nucleic Acids Res*, *47*(W1), W234-W241. https://doi.org/10.1093/nar/gkz240

Figure legends

Figure 1. Hippocampal inflammaging : age-associated sterile inflammation in mouse hippocampus. (A) Volcano plot showing differentially expressed genes in normal aging hippocampus (aged WT PBS versus young WT PBS). Overlapping differentially expressed genes (DEGs) between this comparison and inflammatory response in the young comparison (young WT LPS vs young WT PBS) are identified. Specifically, overlapping DEGs that are downregulated in both comparisons are blue, while upregulated DEGs are in red. (B) Comparison of overlapping gene set enrichment pathways between normal aging and inflammatory response in the young. (C) Hypergeometric testing of DEG overlap between normal aging and inflammatory response in the young. Odds ratio represents strengths of positive association between the two DEG sets. Magnitude of odds ratio is represented by colour key (blue palette) while p-value scoring is labelled (red) (D) Volcano plot showing differentially expressed genes in inflammatory aging hippocampus (aged WT LPS versus young WT LPS). (E) *Left:* Flow cytometry quantification of TSPO protein levels in innate immune cells isolated from brain (MFI, median fluorescence intensity). Microglia (μglia): $CD45^{hi}F4/80^{hi}cd11B^+$; monocytes: $CD45^{int}F4/80^{hi}cd11B^+Ly6c^+MHCII^-$; monocyte-derived macrophages (MF): $CD45^{int}F4/80^{hi}cd11B^+Ly6c^+MHCII^+$. *Right*: Representative histogram of TSPO fluorescence in $CD45^+$ cells isolated from WT and TSPO-KO mouse brain. Statistical tests: 2E: Three-way ANOVA with FDR post-hoc. $P<0.05$.

Figure 2. TSPO-aging interaction in inflammatory transcriptional responses in mouse hippocampus. (A) Volcano plot showing differentially expressed genes in aged WT versus aged TSPO-KO hippocampus at baseline. Differentially expressed genes (DEGs) were either coded in red (significantly upregulated) or blue (significantly downregulated). Significant DEGs are thresholded at FDR <0.05, with upregulation thresholded at Log2FC $\geq$ 0.5 and downregulated at Log2FC$\leq$ -0.5 respectively. (B) *Top:* Effect of TSPO deletion on proportions of brain innate immune cell populations across normal aging. Bottom: Representative gating strategy. Microglia (μglia): $CD45^{hi}F4/80^{hi}cd11B^+$; monocytes: $CD45^{int}F4/80^{hi}cd11B^+Ly6c^+MHCII^-$; monocyte-derived macrophages: $CD45^{int}F4/80^{hi}cd11B^+Ly6c^+MHCII^+$. (C) Volcano plot showing differentially expressed genes in aged WT versus aged TSPO-KO hippocampus following LPS injections. Significant DEGs were thresholded at FDR <0.05 an indicated as orange. DEGs that were reversed in aged compared to young WT vs TSPO-KO hippocampus indicated in blue (significantly downregulated in young but upregulated in aged) and red (significantly upregulated in young, but downregulated in aged) respectively. (D) Fast gene set enrichment analysis (fGSEA) of DEGs in aged WT vs aged TSPO-KO hippocampus following LPS treatment using Gene Ontology Biological Process pathways. Top 5 up- and down-regulated enriched pathways ranked by normalized enrichment score (NES). (E) Comparison of DEG overlap between aged and young WT vs TSPO-KO comparisons using hypergeometric testing. Odds ratio represents strengths of positive association between two DEG sets. Magnitude of odds ratio is represented by colour key (blue palette) while p-value scoring is labelled (red). (F) Effect of TSPO deletion on proportions of brain innate immune cell populations isolated from inflamed aging brain measured by flow cytometry. Representative gating strategy shown in (B). (G-O) Estimation of hippocampal cell-specific contributions to transcriptional signatures detected in LPS treated WT and TSPO-KO mice using CIBERSORTx. Units of the graphs are arbitrary. Data shown as median, interquartile range with error bars indicating minimum and maximum. Statistical tests: Fig 2A, C: Benjamini Hochberg (BH) corrected FDR <0.05; NS, non-significant. Fig 2B: Two-way ANOVA with FDR post-hoc $*p$ <0.05. Fig 2E: Fisher's Exact test to test. Fig 2F:

Two-way ANOVA. Fig 2G-O: Permutational univariate ANOVA, Dunn multiple comparison post-hoc test. **$p < 0.01$. * $p < 0.05$.

Figure 3. Multi WGCNA reveals co-expression network associated with TSPO in aging and inflammaging. (A) Heatmap (*left*) and cluster dendrogram (*right*) showing inter-module relationship among the modules detected. Representation of individual module is defined by the Module Eigengenes (first principal component, PC1, of each module). Heatmap is calculated from the pairwise correlation between every module Eigengene, with intensity as strength of correlation. Hierarchical clustered dendrogram shows eigengene networks, which comprises of one/multiple module Eigengenes). (B - E) Differential expression of modules functionally characterized by gene set enrichment analysis as (B) synaptic maturation module, (C) transcriptional and translational regulation module, (D) cytokine production & adaptive immune responses module, (E) response to bacterium and defense response module, and (F) response to virus module. For each module heatmap of expression of module members for young and aged WT and TSPO-KO samples shown (*left*) and graph of module expression summarized by the module eigengene for each group shown (*right*). Module expression, summarized by the module eigengene, or the PC1, is shown for each group. Eigengene data boxplots are inclusive of its median and interquartile range with error bars indicating minimum and maximum. (G) Integrated transcription factor – module members network of Module 5 (module exclusively upregulated by TSPO-KO Aged group). Edges refer to protein-protein interactions retrieved via STRING database. Orange nodes are the transcription factors whose motifs are significantly enriched (*BH p-adjusted value* <0.05) using Module 5 members as the input list to HOMER software. Yellow nodes refer to first neighbors of the transcription factors within Module 5. Transcription factors which have the highest degree connectivity (protein-protein interactions with the rest of module 5) *NF-Kβ* (e.g. *Rela*) and interferon transcription factors families (e.g *Irf1,Isg15*). Statistical tests: 3A-F: Multivariate PERMANOVA, EMM post-hoc test. * $p < 0.05$. ** $p = 0.02$. *** $p < 0.002$.

Figure 4. Identification of small molecules that transcriptionally phenocopy TSPO-KO hippocampal inflammaging to verify TSPO modulation of NF-κB in senescent microglia. (A) Small molecules identified to transcriptionally phenocopy the TSPO inflammaging signature via Connectivity Mapping. Mean connectivity score against rank of LINCS compounds treated in (A) NPC and (B) GI1 cell line when queried with TSPO inflammaging signature. Positive connectivity score indicates the phenocopying effect of a compound with the query signature, while a negative score indicates the anti-correlation between the compound and query signature. Compounds are ranked in ascending order, from the strongest phenocopy to strongest reversal signal. Green: CDK inhibitors, Pink: HSP90 inhibitors, Yellow: Topoisomerase inhibitors. (C) Quantification of median intensity of SA-β-Gal fluorescence signal (MFI) in cultured WT primary microglia as evaluated by staining of SA-β-Gal. Treatment conditions as follows: VV(Vehicle), EL(Entinostat+LPS), REL (Ro5-4864+Entinostat+LPS). (D) Quantification of nuclear median intensity of NF-kβ immunoreactivity (MFI) in primary microglia. (E) Quantification of sum of total per cell NF-kβ immunoreactivity in primary microglia. (F) Quantification of cellular morphology of the primary microglia as evaluated by whole cell sphericity. (G) Representative confocal images of primary microglia stained for DAPI (blue), NF-kβ (red) and SA-β-Gal (green). Statistical test: Welch One-way ANOVA, FDR post-hoc multiple comparisons. *$p < 0.05$

Figure 5. Effect of TSPO deletion on nuclear NF-kβ activation and cellular senescence in cultured aged macrophages. Immunocytochemistry and staining of SA-β-Gal were performed on cultured macrophages derived from aged WT and TSPO-KO mice. (A) Quantification of nuclear median intensity of NF-kβ immunoreactivity (MFI). (B) Quantification of cellular senescence measured by SA-β-Gal fluorescence (median fluorescence intensity, MFI). (D) Representative confocal images of the cultured macrophages derived from aged WT and TSPO-KO mice. DAPI (blue), NF-kβ (red) and SA-β-Gal (green). Statistics: Welch One-way ANOVA, FDR post-hoc multiple comparisons *$p<0.05$.

Figure 6. Aging and TSPO alter brain metabolic profiles in inflammation. (A) Representative 1D-NOSEY spectra of the 19 metabolites detected in young WT, old WT, young KO and old KO brain tissue samples. Metabolite assignment to NMR peaks indicated. Abbreviation: NAA, N-acetyl aspartate; gln, glutamine; glu, glutamate; Suc, succinate; Tau, taurine; scyIno, scyllo-inositol; mIno, myo-inositol; GPCho, glycerophosphocholine; PCho, phosphocholine; Cho, choline; Cr, creatine; GABA, γ-aminobutyrate; Pyr, pyruvate; Fum, fumarate; AMP, Adenosine monophosphate; ADP, Adenosine diphosphate; ATP, Adenosine triphosphate; Nam, nicotinamide. (B) STOCSY shows high correlation (0.8) between the two singlets (red peaks) at 4.832 (identified in aged TSPO-KO only) and 8.462 ppm, which is formic acid. The correlation suggests that peak at 4.832 could be formaldehyde. Formaldehyde in water presents structure of methanediol and it is a singlet with chemical shift ranging from 4.4-5.4 ppm (Automated Topology Builder (ATB) and Repository Version 3.0, Methanediol | CH4O2 | MD Topology | NMR | X-Ray (uq.edu.au)). (C) Multivariate Dimensionality reduction of targeted NMR metabolites using Partial least squares-discriminant analysis (PLSDA) for young and aged WT and TSPO-KO mice under LPS-induced inflammation. (D) Quantification of metabolites measured by NMR in young and aged brain of WT and TSPO-KO mice under LPS-induced inflammation. Metabolite concentrations shown as median, interquartile range with error bars indicating minimum and maximum. Metabolites that contributed the greatest variance to discrimination of the groups along PC1 are highlighted with black header (aspartate, NAM, NAD, ADP, glutamate, GABA, succinate, fumarate and phosphatidylcholine). Correlation heatmaps show Precursor:Product ratios as measured by Pearsons correlation, with significance threshold $p<0.05$. Precursor:Product metabolite ratios which showed significant changes during aging were Fumarate:Succinate, and Glutamine:Glutamate (Fumarate:Succinate and Glutamine:Glutamate significantly correlated in the Young but not Aged). Conversely, Glutamate:GABA ratio showed significant correlation exclusively in the TSPO Aged group.

Supplementary Fig. 1. Cell-type contributions to hippocampal aging transcriptomic signatures in WT & TSPO-KO mice. Estimation of hippocampal cell-specific contributions to aging transcriptional signatures in WT and TSPO-KO mice under baseline conditions. Units of the graphs are arbitrary. Data shown as median, interquartile range with error bars indicating minimum and maximum. Statistical tests: Two-way ANOVA. * $p < 0.05$.

Supplementary Fig. 2. PPI interaction subnetwork of immune (*top*) and transcriptional-translational processes (*bottom*) derived from the module driver genes of Module 3 identified by multiWGCNA.

Supplementary Fig. 3. PPI subnetwork of immune-related transcription factors and helicases in Module 4 genes identified by multiWGCNA.

Supplementary Fig. 4 . Effect of TSPO deletion on nuclear NF-kβ activation and cellular senescence in cultured aged macrophages. (A) uantification of sum of per cell NF-kβ immunoreactivity in primary cultured macrophages. (B) Quantification of cellular morphology

of the cultured macrophages as evaluated by whole cell sphericity. Values closer to 1.0 have higher sphericity while lower values represent ellipticity. (C) Quantification of senescence associated heterochromatic foci (SAHF) in cultured macrophages measured by punctate DAPI staining.

Supplementary Table 1A Differentially expressed gene list for normal aging. Comparison is between WT Aged vs WT Young (reference) under baseline (PBS) conditions. Significance is defined as FDR<0.05. Upregulation refers to significant genes thresholded at Log2FC $\geq$ 0.5, while downregulation refers to significant genes thresholded at Log2FC $\leq$ -0.5.

Supplementary Table 1B fGSEA functional enrichment results from differentially expressed genes of normal aging comparison (Supplementary Table 1A) NES score refers to normalized enrichment score. Leading edge refers to genes annotated with their Entrez IDs being involved in that functional term.

Supplementary Table 1C fGSEA leading edges with gene symbols from Supplementary Table 1B) NES score refers to normalized enrichment score. MGI refers to the overlapping genes involved in the functional term.

Supplementary Table 1D Gene overlap hypergeometric Fischer tests of significant differentially expressed genes between normal aging and inflammatory response in the young. WT PBS Aged vs WT PBS Young is denoted as the normal aging comparison, while WT LPS Young vs WT PBS Young is denoted as the inflammatory response in the young comparison. Each significant differentially expressed gene set is split into either upregulated 'up' (Log2FC >0.5) or downregulated 'down' (Log2FC <0.5). Magnitude of overlap is reflected as odds ratio, while significance threshold is p<0.05 for the hypergeometric Fischer test.

Supplementary Table 1E fGSEA functional enrichment results from differentially expressed genes of inflammatory response in the young. NES score refers to normalized enrichment score. Leading edge refers to genes annotated with their Entrez IDs being involved in that functional term.

Supplementary Table 1F Differentially expressed gene list for inflammation in the aged brain Comparison is between WT LPS Aged vs WT PBS Aged conditions. Significance is defined as FDR<0.05. Upregulation refers to significant genes thresholded at Log2FC $\geq$ 0.5, while downregulation refers to significant genes thresholded at Log2FC $\leq$ -0.5.

Supplementary Table 1G Differentially expressed gene list for aging in the inflamed hippocampi. Comparison is between WT LPS Aged vs WT LPS Young conditions. Significance is defined as FDR<0.05. Upregulation refers to significant genes thresholded at Log2FC $\geq$ 0.5, while downregulation refers to significant genes thresholded at Log2FC $\leq$ -0.5.

Supplementary Table 2A Differentially expressed gene list for the effect of TSPO deletion in the aged brain Comparison is between KO PBS Aged vs WT PBS Aged conditions. Significance is defined as FDR<0.05. Upregulation refers to significant genes thresholded at Log2FC $\geq$ 0.5, while downregulation refers to significant genes thresholded at Log2FC $\leq$ -0.5.

Supplementary Table 2B Differentially expressed gene list for the effect of TSPO deletion in the inflamed aged brain Significant (FDR<0.05) differentially expressed genes TSPOKO

LPS Aged vs WT LPS Aged. Upregulation refers to significant genes thresholded at Log2FC ≥ 0.5, while downregulation refers to significant genes thresholded at Log2FC ≤ -0.5.

Supplementary Table 2C fGSEA functional enrichment results from differentially expressed genes evaluating the effect of TSPO deletion in the aged brain . Gene input is based on all differentially expressed genes comparing TSPOKO Aged vs WT Aged. NES score refers to normalized enrichment score. MGI refers to the overlapping genes involved in the functional term.

Supplementary Table 2D Gene overlap hypergeometric Fischer tests comparing the effect of TSPO deletion across aging of the inflamed brain. Gene overlap is performed to compare overlapping differentially expressed genes between TSPOKO LPS Aged vs WT LPS Aged comparison and TSPOKO LPS Young vs WT LPS Young comparison. Each significant differentially expressed gene set is split into either upregulated 'up' (Log2FC >0.5) or downregulated 'down' (Log2FC <0.5). Magnitude of overlap is reflected as odds ratio, while significance threshold is $p<0.05$ for the hypergeometric Fischer test.

Supplementary Table 2E Functional enrichment of the markers belonging to the sub categories of cell types Sub categories of cell types detected via deconvolution of our bulk RNAseq dataset expression matrix using (Zeisel et al., 2015). Markers are derived using Seurat by comparing each subcategory of cell type against all other subcategories using `FindMarkers` function.

Supplementary Table 3A. Module Eigengenes calculated for each module. Module Eigengenes (PC1) calculated for each module, based on expression. Includes sample metadata for mapping sample groups, and the pairwise marginal means (emmeans) for post-hoc analysis after PERMANOVA.

Supplementary Table 3B. Over representation Gene Ontology functional enrichment of significant modules (Module 1-6). Gene Ontology functional enrichment using C5 of MsigDb. Overlap genes shows module genes involved in the functional term. Overlap represents size of overlap genes while size represents size of the gene set. Significance is determined by FDR p.adjusted value (padj<0.05).

Supplementary Table 3C. Intra-module connectivity of module members. All module members, and the respective size of each module is documented. Next, members with high intra-module connectivity (where gene members >0.9 correlation with PC1 of module, were filtered out.

Supplementary Table 3D. Transcription factors enriched are predicted from Module 5 via HOMER Motif analysis. Transcription factors that are significantly enriched from module 5 members' promoters (Benjamini Hochberg p adjusted value<0.05) are selected. Cognate genes from these transcription factors are isolated from the expression matrix, and integrated with Module 5 members as a Network. Network are derived via Network Analyst website, by querying through STRING database for PPI. Network topology is documented with details of describing Hub genes measurement such as degree (number of PPI interactions) and Betweenness Centrality (measure of centrality of gene within network).

Supplementary Table 4. Connectivity Map query of the top 100 differentially expressed genes in TSPOKO inflammaging. Querying is conducted via (Zhang & Gant, 2008) method in either Neural precursor cell line (NPC) or Glioblastoma cell line (Gli1). Maximal phenocopy

or reversal of transcriptional signature is +1 or -1 of the mean connectivity score respectively. Smaller rank magnitude represents a transcriptional phenocopy while larger rank magnitude represents a transcriptional reversal.
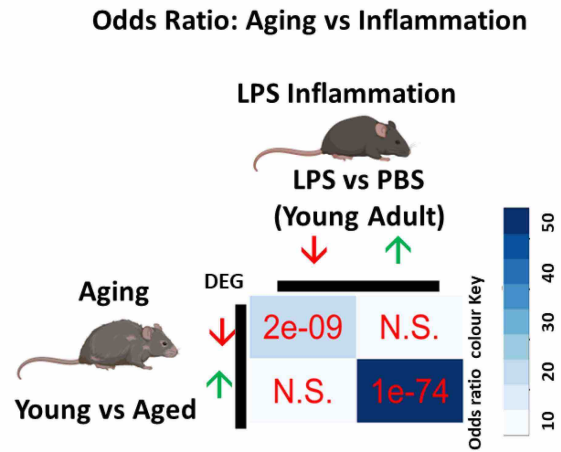
Figure 1

Hippocampal inflammaging : age-associated sterile inflammation in mouse hippocampus
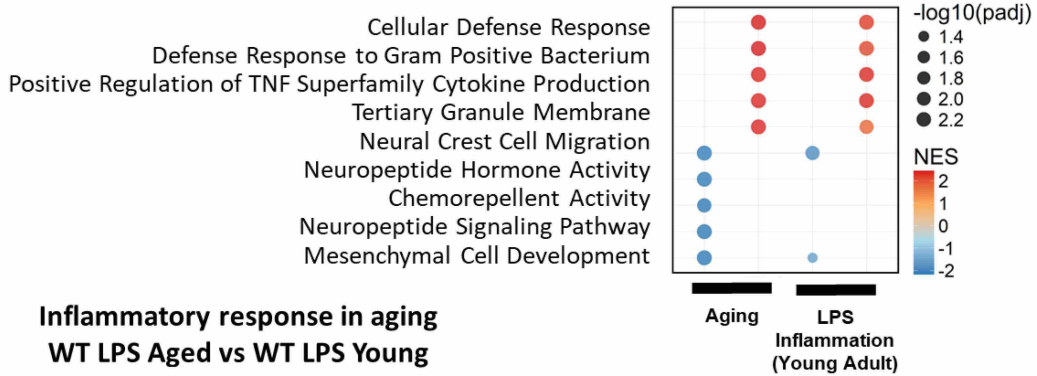

(A) Normal aging WT Aged vs WT Young
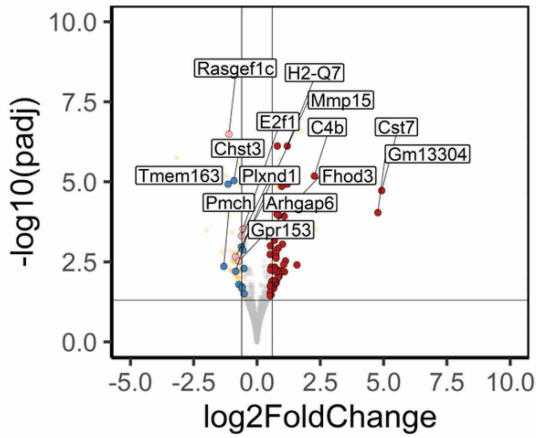
- DEG
- ↓ Normal aging ↓ Young Inflammatory response
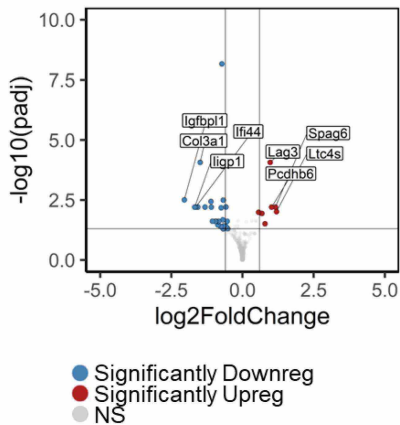- ↑ Normal aging ↑ Young inflammatory response
- ↓ Normal aging ↑ Old inflammatory response
- NS

(C) Odds Ratio: Aging vs Inflammation

(B) Transcriptional pathways affected by aging overlap with LPS-induced inflammatory pathways

(D) Inflammatory response in aging WT LPS Aged vs WT LPS Young

- Significantly Downreg
- Significantly Upreg
- NS

(E) Aging decreases TSPO expression in brain innate immune cells
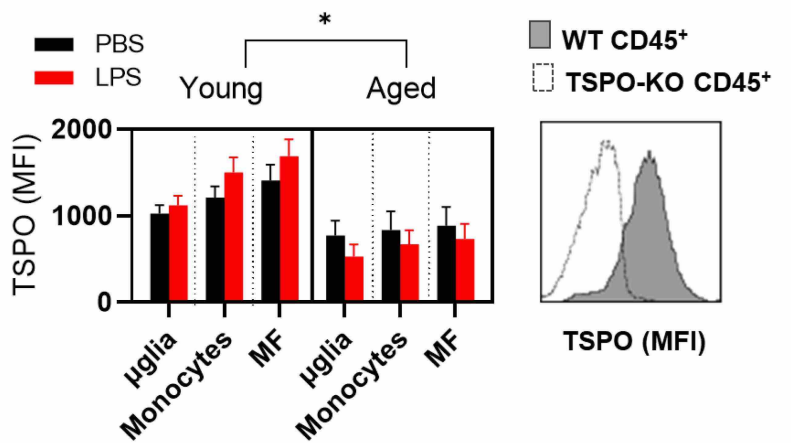
Figure 2

Hippocampal inflammaging is TSPO-independent

(A) **TSPO in Inflammaging Aged WT vs Aged TSPO-KO**

(B) **Effect of TSPO-KO on innate immune cell populations in aging brain**

TSPO - aging interaction in inflammatory transcriptional responses in hippocampus

(C) **Inflammatory responses in aging WT vs TSPO-KO**

(E) **Odds Ratio: WT vs TSPO-KO**

(D) **Transcriptional pathways affected by TSPO-KO in inflamed aging hippocampus**

- NADH Dehydrogenase Complex
- NADH Dehydrogenase Complex Assembly
- ATP synthesis coupled e- transport
- Respirasome
- GABAergic synpase
- Defense response to symbiont
- Cell activation involved in immune response
- Positive regulation of TNFSF cytokine production
- Positive regulation of IL-6 production
- Response to TNF

(F) **Effect of TSPO-KO on brain innate immune cell populations in inflamed aging brain**

Effect of TSPO on cell-type contributions to hippocampal inflammatory transcriptomic signatures in aging brain
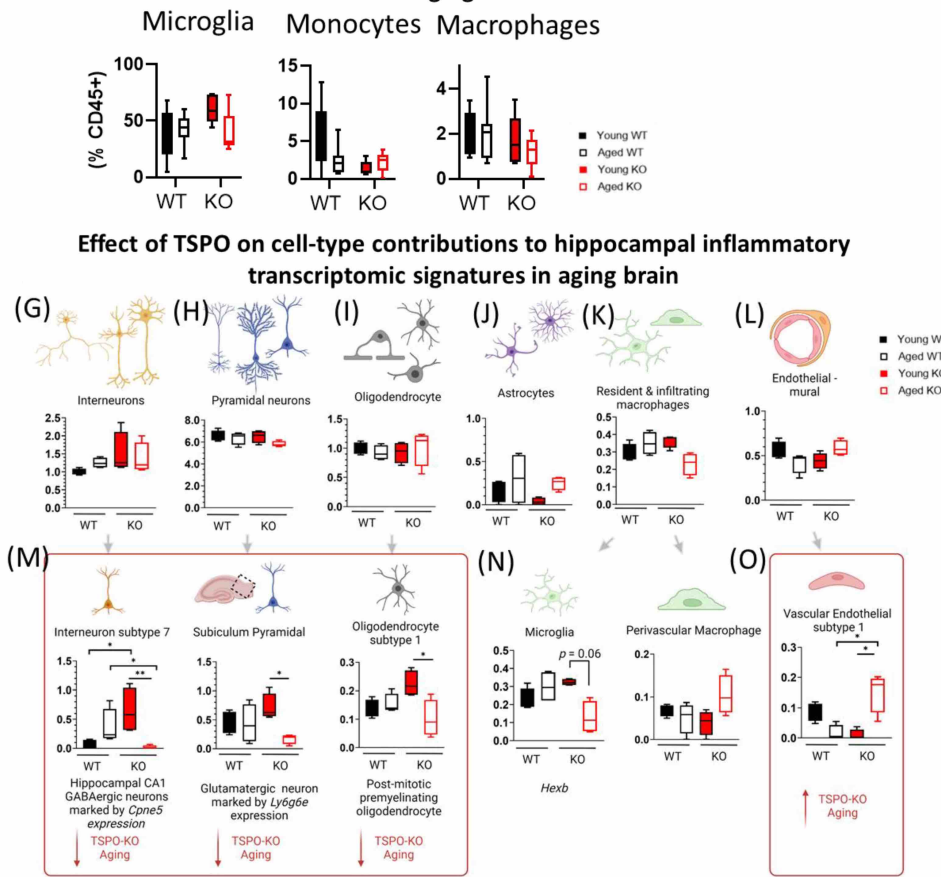
Figure 3

(A)

Correlation between modules

Inter-module higher organization

Innate immunity   Immunity & defense   Synaptic maturation   Metabolic processes
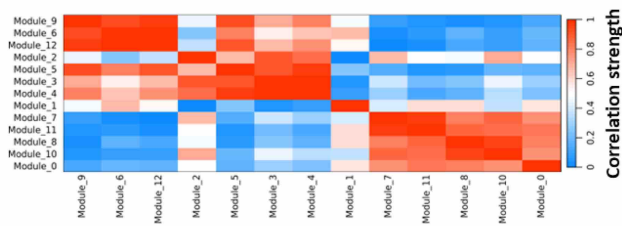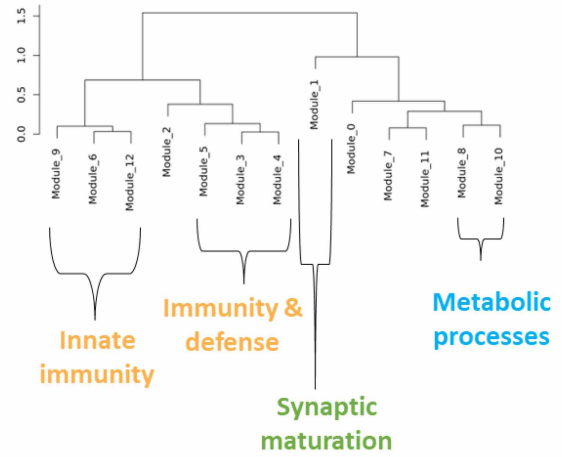
Age-associated co-expression modules

(B) Synaptic Maturation

↓ Aging
↓ TSPO-KO
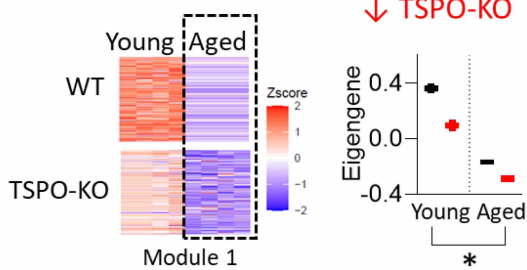
Module 1

(C) Immunity & Transcriptional Regulation

↑Aging
↑ TSPO-KO
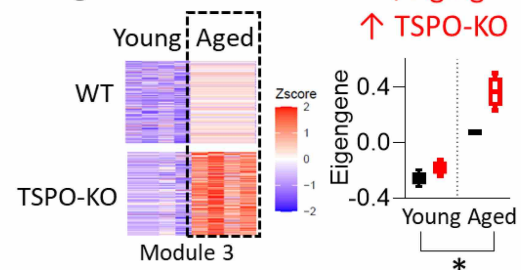
Module 3

TSPO-aging interaction co-expression modules

(D) Cytokine Production & Adaptive Immune Responses

↑Aging
↑ ↑ TSPO-KO Aging
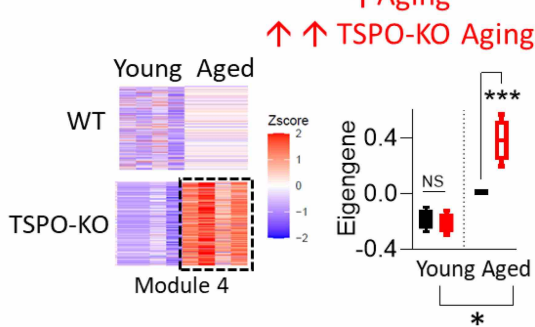
Module 4

(E) Response to bacterium and defence response

↑ TSPO-KO Aging

Module 5

(F) Response to Virus

↓ WT Aging
↑ TSPO-KO Aging

Module 6

(G)
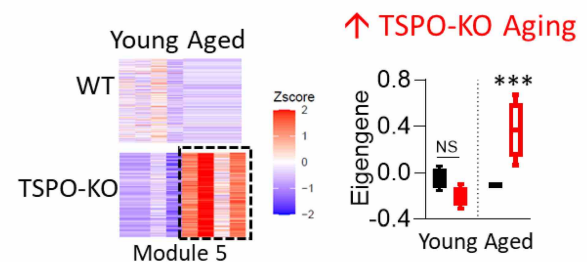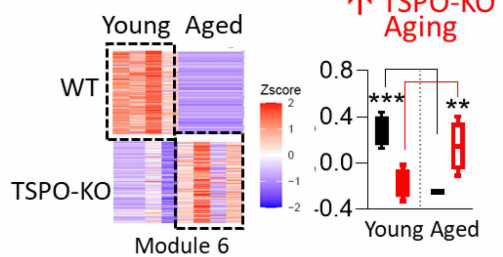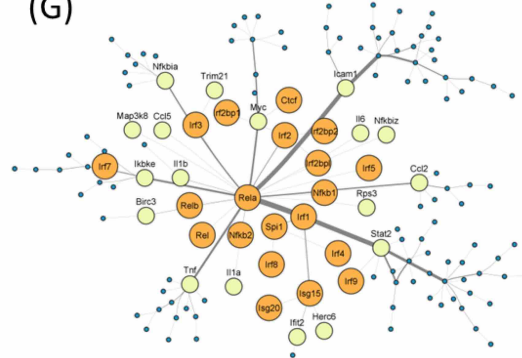
● Transcription factors detected
● First neighbours of transcription factors
● Module 5 members

Figure 4
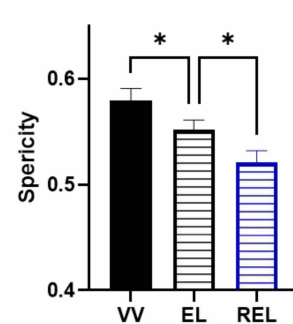## Small molecules phenocopying TSPO inflammaging transcriptional signature
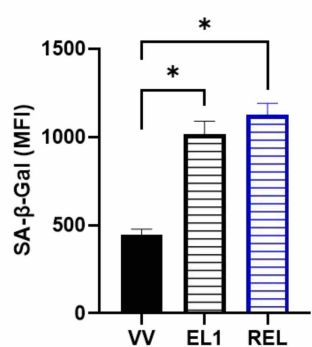
(A) *NPC*

(B) *GI1*

Transcriptional Phenocopy

Transcriptional Reversal

Drug MOA

- ● CDK inhibitor
- ● HSP inhibitor
- ● Topoisomerase inhibitor

(C) Cellular Senescence

(D) Nuclear NF-Kβ
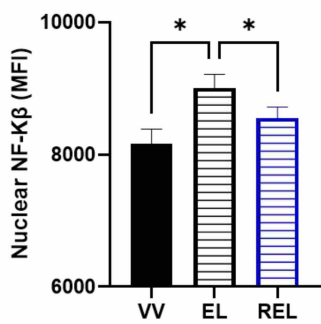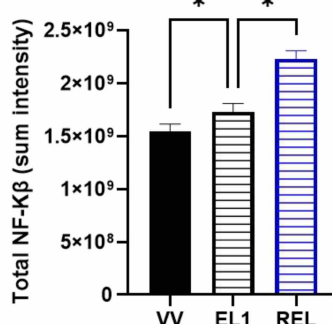
(E) Total NF-Kβ

(F) Macrophage morphology

(G)

Entinostat + LPS

Ro5-4864 + Entinostat + LPS

Figure 5

(A)

NFKB

Nuclear NFkB (MFI)

8000
6000
4000
2000
0

| LPS | - | + | - | + | - | + | - | + |
| Entinostat | - | - | + | + | - | - | + | + |

WT   TSPO-KO

(B)

Cellular Senescence

SA-β-Gal (MFI)

500
400
300
200
100
0

| LPS | - | + | - | + | - | + | - | + |
| Entinostat | - | - | + | + | - | - | + | + |

WT   TSPO-KO

(C)

WT

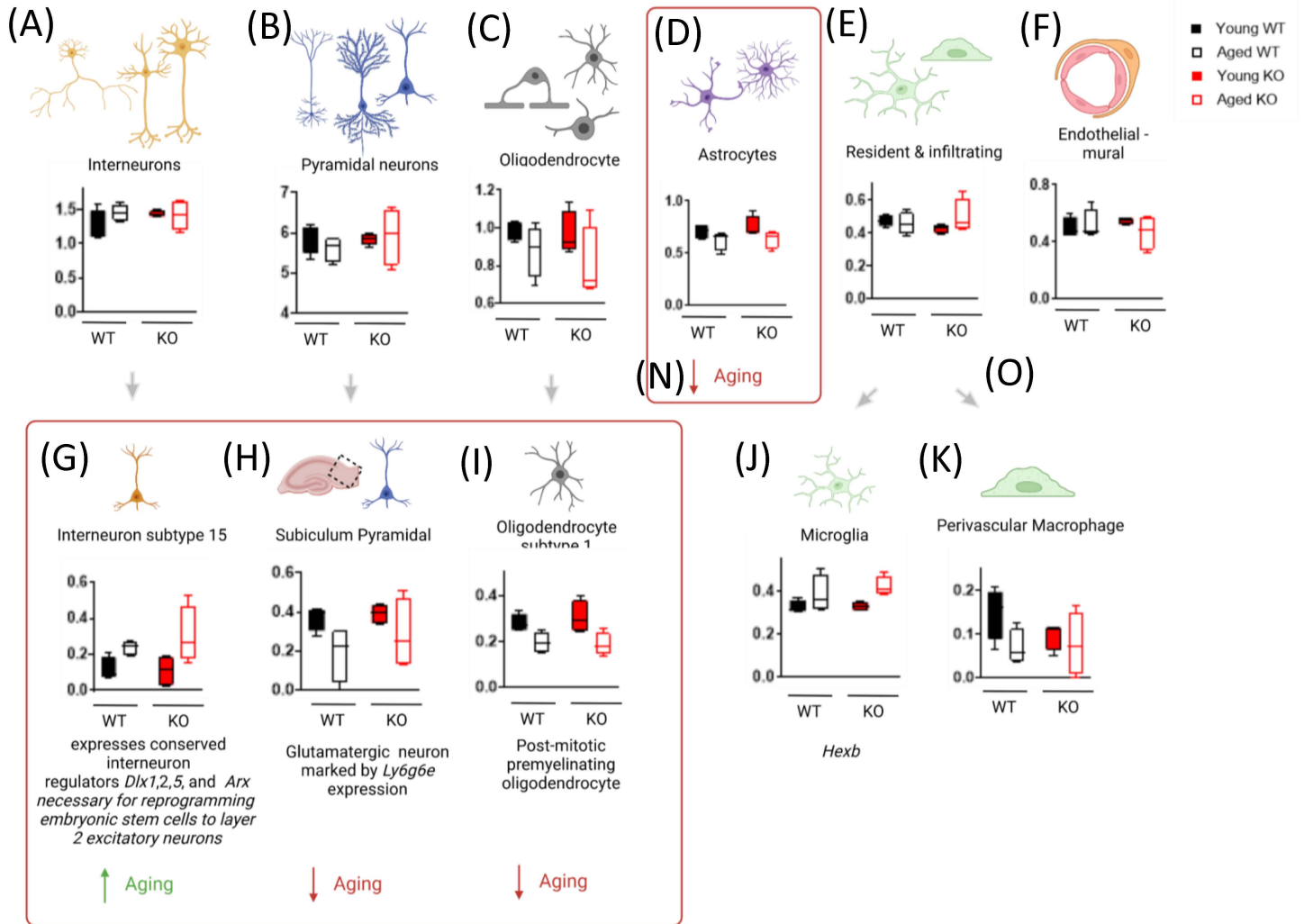WT + LPS

TSPO-KO

TSPO-KO + LPS
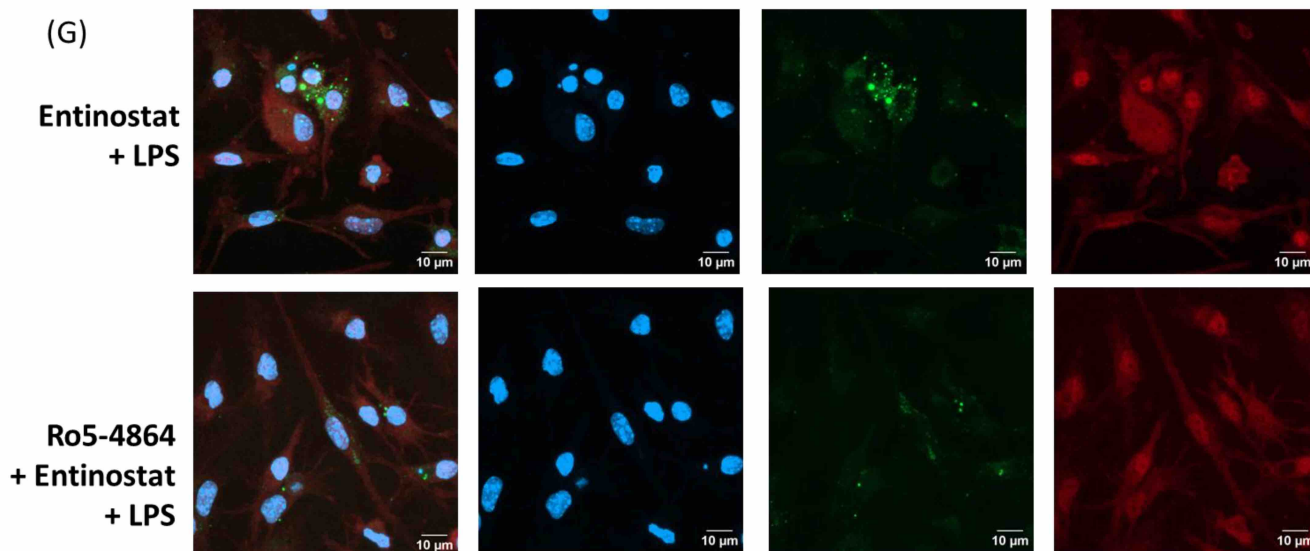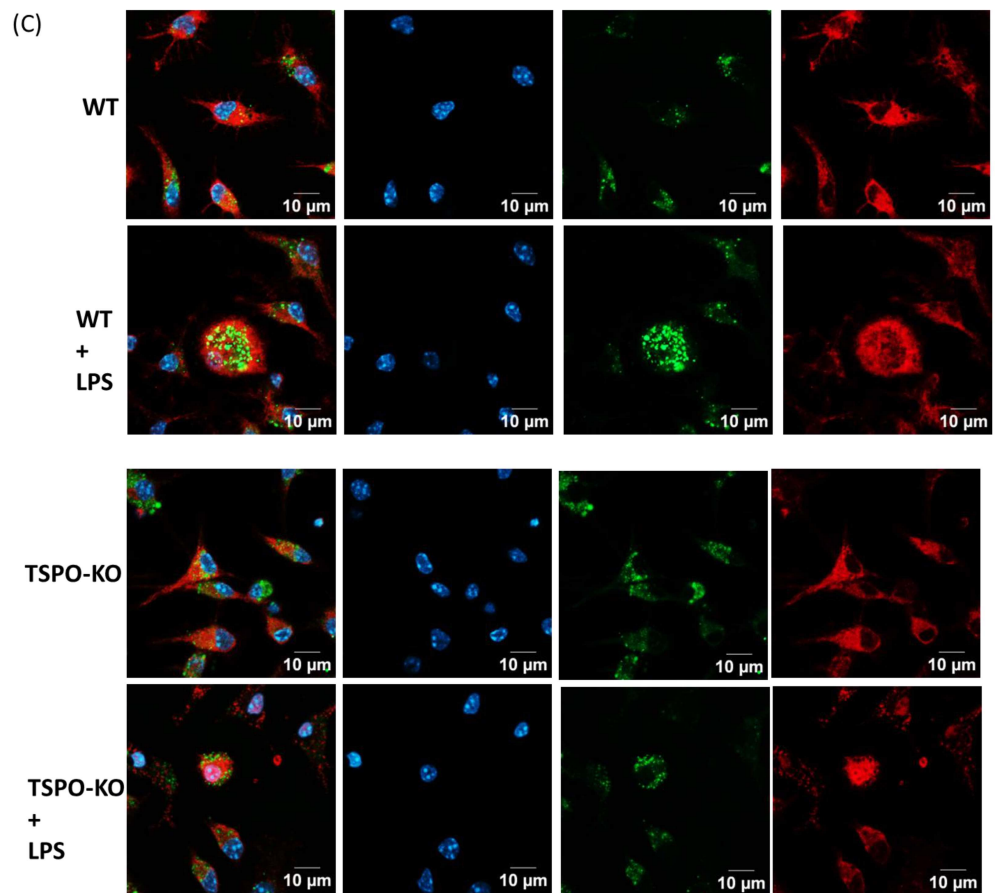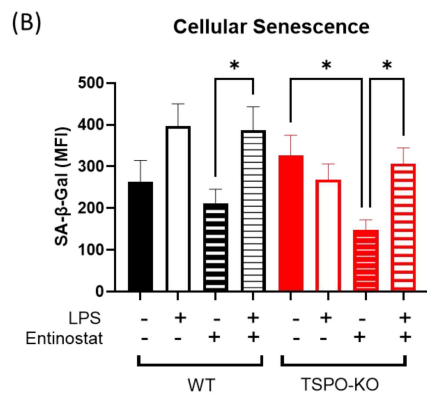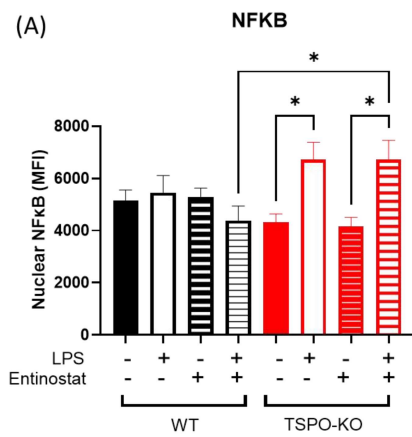
Figure 6   Aging and TSPO alter brain metabolic profiles in inflammation
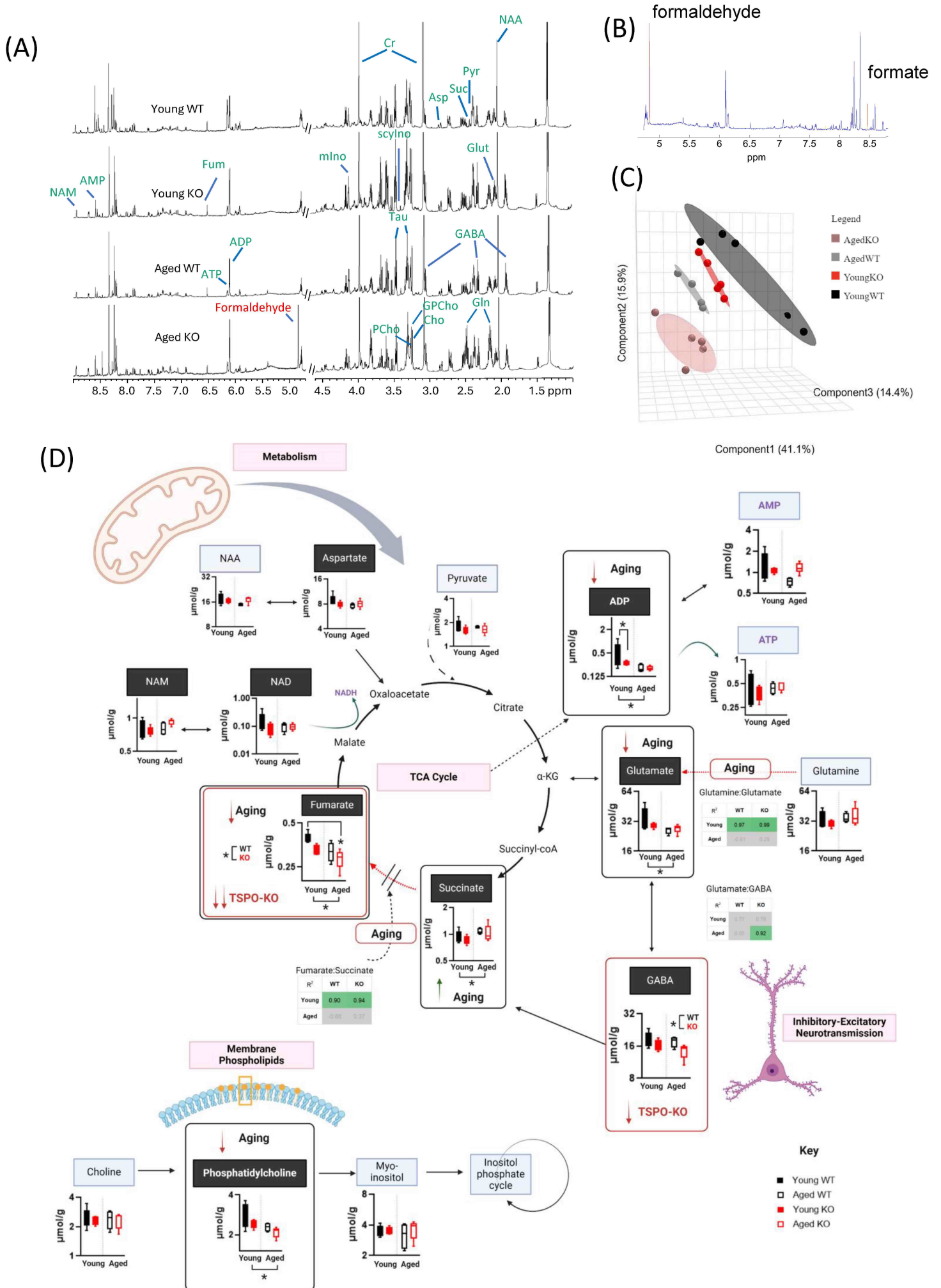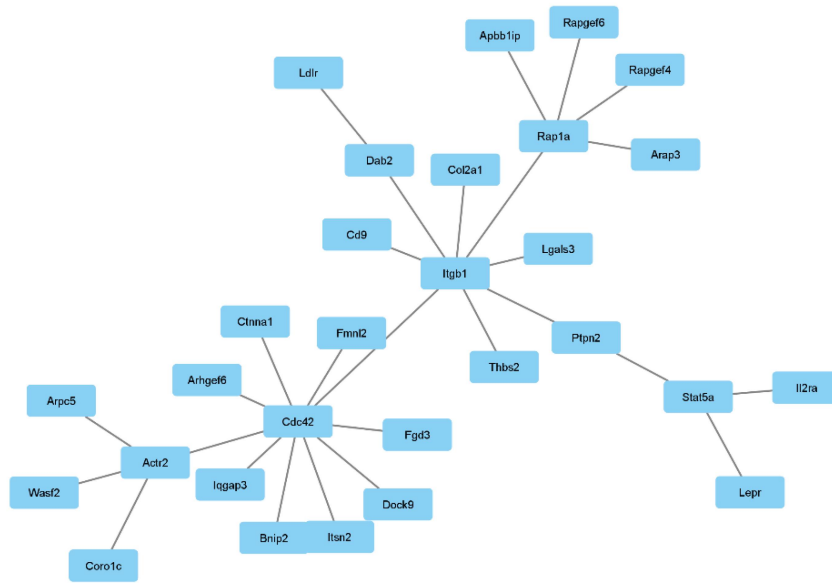
Suppl. Fig 1

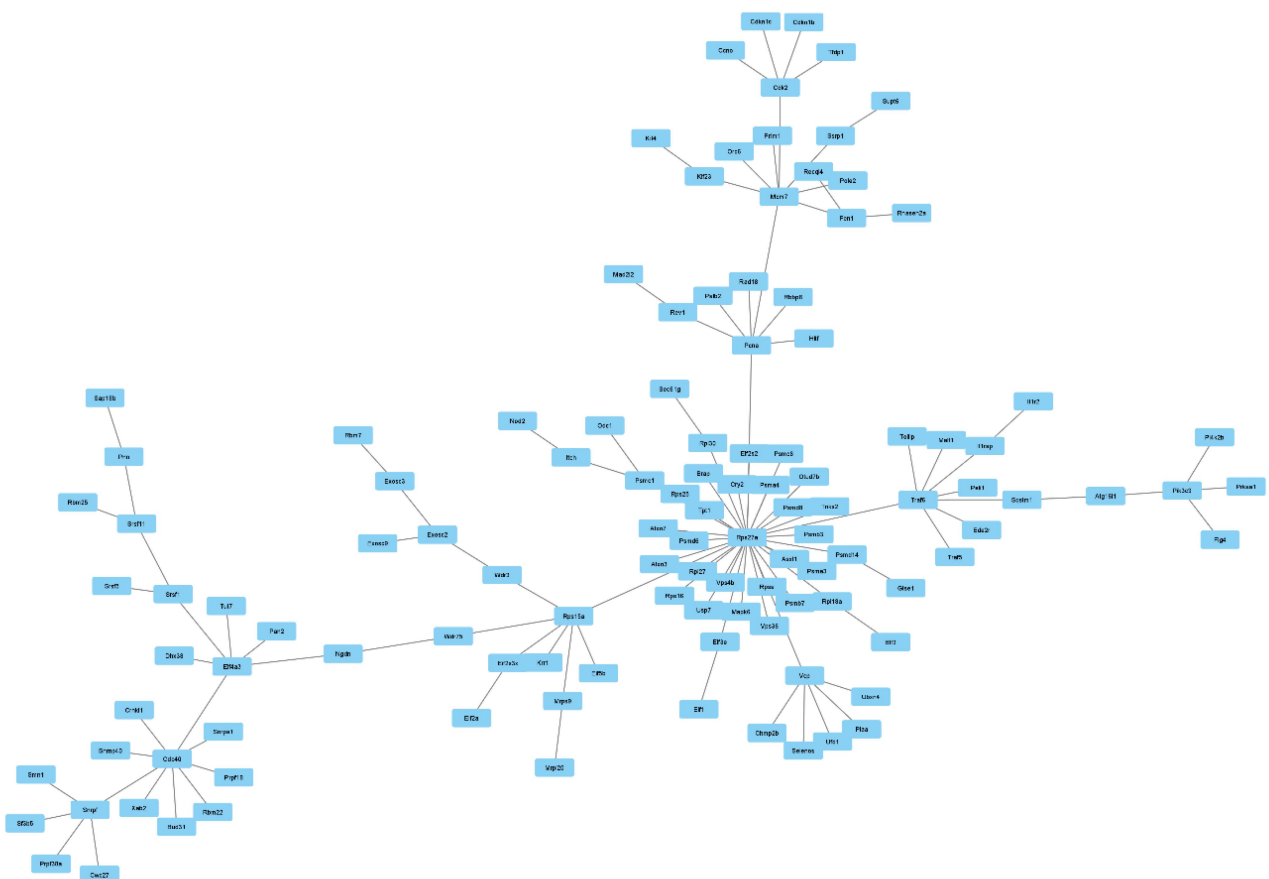Cell-type contributions to hippocampal aging transcriptomic signatures in WT & TSPO-KO mice

Immune subnetwork of PPI interactions derived from the module driver genes of Module 3

Transcriptional-Translational processes subnetwork of PPI interactions derived from the module driver genes of Module 3

Suppl. Fig 3

Immune related transcription factors and helicases PPI subnetwork of Module 4.

Suppl. Fig 4

(A)

Whole Cell NFKB

(B)

Macrophage morphology

(C)

Heterochromatin Foci